# Hindering the applicability of the authigenic 10Be/9Be dating by redeposition of mud in hybrid event beds, eastern Danube Basin, Slovakia

Michal Šujan, Kishan Aherwar, Katarína Šarinová, Tomáš Vlček, Andrej Chyba, Natália Hudáčková, Michal Jamrich, Marianna Kováčová, Orsolya Sztanó

▶ **To cite this version:**

Michal Šujan, Kishan Aherwar, Katarína Šarinová, Tomáš Vlček, Andrej Chyba, et al.. Hindering the applicability of the authigenic 10Be/9Be dating by redeposition of mud in hybrid event beds, eastern Danube Basin, Slovakia. Applied Geochemistry, In press, pp.106254. 10.1016/j.apgeochem.2024.106254 . hal-04840255

**HAL Id: hal-04840255**
**https://hal.science/hal-04840255v1**

Submitted on 16 Dec 2024

**HAL** is a multi-disciplinary open access archive for the deposit and dissemination of scientific research documents, whether they are published or not. The documents may come from teaching and research institutions in France or abroad, or from public or private research centers.

L'archive ouverte pluridisciplinaire **HAL**, est destinée au dépôt et à la diffusion de documents scientifiques de niveau recherche, publiés ou non, émanant des établissements d'enseignement et de recherche français ou étrangers, des laboratoires publics ou privés.

Copyright

# Journal Pre-proof

Hindering the applicability of the authigenic $^{10}Be/^{9}Be$ dating by redeposition of mud in hybrid event beds, eastern Danube Basin, Slovakia

Michal Šujan, Kishan Aherwar, Katarína Šarinová, Tomáš Vlček, Andrej Chyba, Natália Hudáčková, Michal Jamrich, Marianna Kováčová, AsterTeam, Orsolya Sztanó

PII: S0883-2927(24)00359-7

DOI: https://doi.org/10.1016/j.apgeochem.2024.106254

Reference: AG 106254

To appear in: *Applied Geochemistry*

Received Date: 6 October 2024

Revised Date: 27 November 2024

Accepted Date: 9 December 2024

Please cite this article as: Šujan, M., Aherwar, K., Šarinová, K., Vlček, T., Chyba, A., Hudáčková, N., Jamrich, M., Kováčová, M., AsterTeam, Sztanó, O., Hindering the applicability of the authigenic $^{10}Be/^{9}Be$ dating by redeposition of mud in hybrid event beds, eastern Danube Basin, Slovakia, *Applied Geochemistry*, https://doi.org/10.1016/j.apgeochem.2024.106254.

This is a PDF file of an article that has undergone enhancements after acceptance, such as the addition of a cover page and metadata, and formatting for readability, but it is not yet the definitive version of record. This version will undergo additional copyediting, typesetting and review before it is published in its final form, but we are providing this version to give early visibility of the article. Please note that, during the production process, errors may be discovered which could affect the content, and all legal disclaimers that apply to the journal pertain.

© 2024 Published by Elsevier Ltd.

Journal Pre-proof

# Hindering the applicability of the authigenic $^{10}Be/^{9}Be$ dating by redeposition of mud in hybrid event beds, eastern Danube Basin, Slovakia

Michal Šujan[1,2]*, Kishan Aherwar[2], Katarína Šarinová[3], Tomáš Vlček[2], Andrej Chyba[4], Natália Hudáčková[2], Michal Jamrich[2], Marianna Kováčová[2], AsterTeam[5], Orsolya Sztanó[6]

[1] *Laboratory of Quaternary Research, Nature Research Centre, Akademijos g. 2, LT-08412 Vilnius, Lithuania; michal.sujan@gamtc.lt*

[2]*Department of Geology and Paleontology, Faculty of Natural Sciences, Comenius University in Bratislava, Ilkovičova 6, 842 15 Bratislava, Slovakia; michal.sujan@uniba.sk*

[3]*Comenius University Bratislava, Faculty of Natural Sciences, Department of Mineralogy, Petrology and Economic Geology, Ilkovičova 6, 842 15 Bratislava, Slovakia*

[4]*Institute of Chemistry, Slovak Academy of Sciences, Dúbravská cesta 9, 845 38 Bratislava, Slovakia; andrej.chyba@savba.sk*

[5]*CNRS-IRD-Collège de France-INRA, CEREGE, Aix-Marseille Univ., 13545 Aix-en-Provence, France*

[6]*Eötvös Loránd University, Department of Geology, Pázmány Péter sétány 1/C, 1117 Budapest, Hungary*

* – corresponding author

## Abstract

The authigenic $^{10}Be/^{9}Be$ dating method is a relatively new geochronological technique that shows great potential for use in epicontinental sedimentary successions, largely due to its ability to date ubiquitous mud. However, the factors influencing the applicability of this method are not yet fully understood, which limits its robust application. This study presents the first direct

evidence that deep-water mud redeposition can lead to significantly older authigenic $^{10}Be/^{9}Be$ ages, with an offset of ca. 2 Myr in the studied example. The redeposition generated hybrid event beds (products of mixed gravity flows) on the Late Miocene basin floor of Lake Pannon. The source material for redeposition was the Middle Miocene successions exposed on the lake bottom, as indicated by reworked foraminiferal and calcareous nannoplankton fossils, as well as inorganic and organic geochemical proxies. This case study suggests that a thorough understanding of depositional processes and paleogeographic settings is essential when proposing future authigenic $^{10}Be/^{9}Be$ dating sampling strategies, to avoid the influence of deep-water mud redeposition by hybrid event beds. Additionally, a notable shift in geochemical signature was observed between syn- and post-rift phases. During the ca. 6 Myr-long rifting, sediment recycling and local provenance were dominant from the rifted basin margins, while the post-rift stage marked the onset of a regional-scale sediment routing system. Notably, organic matter preserved its compositional signature of the redeposited successions.

**Key words:** geochronology; cosmogenic nuclides; meteoric $^{10}Be$, epicontinental basin; Miocene; Central Europe

## Graphical abstract

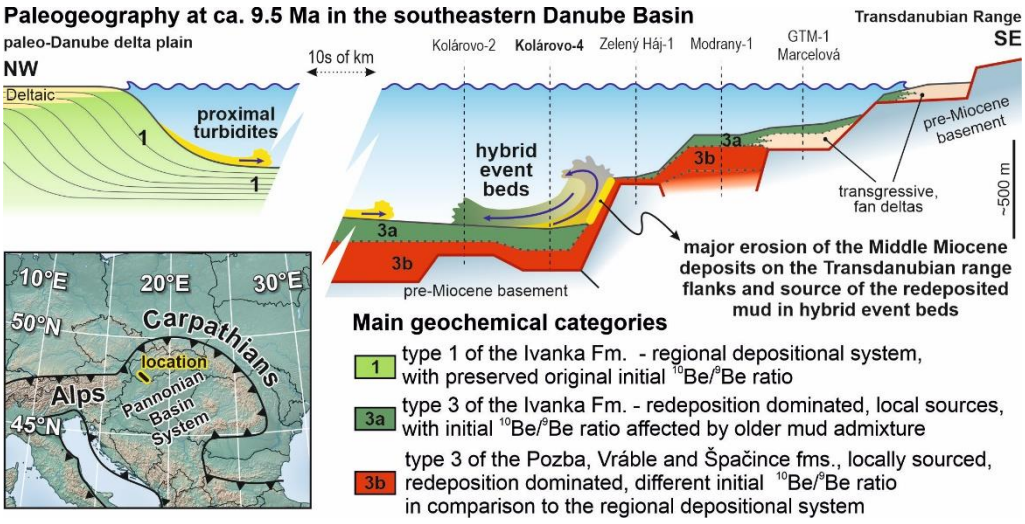

## 1. Introduction

The authigenic $^{10}Be/^{9}Be$ dating method shows great potential in geochronology thanks to its ability to date the deposition of clay-bearing sediment, the most common type of deposit on Earth (Schieber, 1998).This is even underlined by the theoretical range of the method's applicability reaching ~0.2–14 Ma (e.g., Bourlès et al., 1989; Lebatard et al., 2008), implied by the half-life of $^{10}Be$ with the value of 1.378 ± 0.012 Ma (Chmeleff et al., 2010; Korschinek et al., 2010). However, the limitations of the method are not yet fully appreciated, as only 51 studies have been published utilizing the authigenic $^{10}Be/^{9}Be$ ratio in geochronology since 1982, and only 20 of these focused on depositional histories in epicontinental basins, published from 2005 onward (Šujan, 2024).

The major issue to be solved is the identification and understanding of the factors affecting the variability of the initial authigenic $^{10}Be/^{9}Be$ in sedimentary environments, which reaches the range of ~1.4–193 × $10^{-9}$ across oceanic settings (e.g., Krishnaswami et al., 1982; Measures and Edmond, 1982; Sharma and Somayajulu, 1982; Kusakabe and Ku, 1984; Kusakabe et al., 1987; Sharma et al., 1987; Bourlès et al., 1989; Brown et al., 1992b; Measures et al., 1996; Aldahan et al., 1997; von Blanckenburg and O'Nions, 1999; Nagender Nath et al., 2007; Willenbring and Von Blanckenburg, 2010a; Jena et al., 2022; 2023a, b) and spans from ~0.5 × $10^{-9}$ to 230 × $10^{-9}$ across shallow marine, deltaic, lacustrine, alluvial and loess settings and in soils (e.g., Brown et al., 1992a; Barg et al., 1997; Graham et al., 1998; 2001; McHargue et al., 2011; Wittmann et al., 2018; Portenga et al., 2019; Simon et al., 2019; Balco et al., 2021; Lisé-Pronovost et al., 2021; Suhrhoff et al., 2022; Jeong et al., 2023; Aherwar et al., 2024). The considerable fluctuation is inherently associated with different source of the two isotopes, since radioactive $^{10}Be$ is produced in the atmosphere by interaction of $^{14}N$ and $^{16}O$ with cosmic rays, while stable $^{9}Be$ is supplied by chemical weathering of rocks. Both isotopes are incorporated in Fe and Mn oxyhydroxides, forming authigenic rims around sedimentary particles in a water

column, which are the target of the dating method (Bourlès et al., 1989; Willenbring and von Blanckenburg, 2010b; Wittmann et al., 2012; Singleton et al., 2017). Assuming a chemically closed system after sedimentation, the change of the authigenic $^{10}Be/^{9}Be$ in the oxyhydroxide rim due to the radioactive decay of $^{10}Be$ can be used to quantify a depositional age (Bourlès et al., 1989).

Several effects driving the initial $^{10}Be/^{9}Be$ ratio in sedimentary environments were already proposed or described. The additive effect, as presented by Willenbring and von Blanckenburg (2010b), was shown to cause a relative increase of $^{10}Be$ input into a maar lake due to the intensification of East Asian monsoon (Cao et al., 2023). Despite the proposed averaging of $^{9}Be$ delivery in large river catchments (von Blanckenburg et al., 2012), the varying petrographic composition affected the resulting isotopic ratios in Ganga and Po river catchments (Rahaman et al., 2017; Aherwar et al., 2024). A significant increase of recent $^{10}Be/^{9}Be$ through a transition from deltaic to open ocean settings (Wittmann et al., 2017; Kong et al., 2021; Jena et al., 2023b) is likely associated with mixing of riverine waters enriched by terrigenous $^{9}Be$ with basinal waters having relatively higher $^{10}Be/^{9}Be$ ratios (Brown et al., 1992b). A $^{10}Be$ enrichment of shelfal sediment may result from condensed deposition, possibly after deltaic avulsion (Barg et al., 1997; Aherwar et al., 2021). On the other hand, diagenetic release of beryllium into pore waters and its precipitation in the near-bed sediment may significantly alter the isotopic ratio preserved in the depositional record (Deng et al., 2023). Terrestrial systems with low rate of deposition and burial could be affected by increased input of $^{10}Be$ from meteoric waters during pedogenesis (Dixon et al., 2018; Šujan et al., 2023a). Rivers under settings of a falling erosional base are prone to incision and redeposition of older mud, presence of which decreases the apparent initial $^{10}Be/^{9}Be$ ratio and increases the radiometric age (Šujan et al., 2023b).

Redeposition of mud was supposed to cause apparently older authigenic $^{10}Be/^{9}Be$ ages also in the Upper Miocene deep-water depositional systems of the Danube Basin, Pannonian Basin

System (Šujan et al., 2016). In this case study, we aimed to verify this process using a multiproxy analysis of the depositional record. We compare the authigenic $^{10}Be/^{9}Be$ signature in a deep-water succession deposited on the basin floor of Lake Pannon by gravity currents with the isotopic record from the underlying Middle Miocene marine deposits of the Central Paratethys Sea, analyzed in the cores of the Kolárovo-4 well (Fig. 1B, D). The Pannonian succession yields authigenic $^{10}Be/^{9}Be$ ages significantly older when compared to the established chronostratigraphy (e.g., Sztanó et al., 2016a). We integrate sedimentological, biostratigraphic and geochemical proxies with the aim to evaluate the processes and role of redeposition in deep-water epicontinental basin settings as a factor affecting the authigenic $^{10}Be/^{9}Be$ dating. The relative change in the initial $^{10}Be/^{9}Be$ ratios is possible to evaluate thanks to the previously established and verified lacustrine initial ratio (Šujan et al., 2016). The study builds upon the findings of the paleoenvironmental investigation of the same succession done by Vlček et al. (2024). This study highlights the necessity of a precise evaluation of depositional processes, which formed a succession to be dated to obtain trustworthy authigenic $^{10}Be/^{9}Be$ ages.

## 2. Geological settings

The Danube Basin is a northwesternmost depocenter of the Pannonian Basin System (PBS) in Central Europe, located between the Eastern Alps, Western Carpathians and Transdanubian Mts. (Horváth et al., 2006) (Fig. 1A). The basin fill was formed during four phases of back-arc basin rifting, during which repeated transgressions of marine or brackish water bodies appeared (Šujan et al., 2021b). The first three occurred in the Central Paratethys Sea with temporally changing connectivity to the neighboring Mediterranean and Black Sea basins, and the fourth one appeared as the biggest lake in the late Cenozoic history of Europe – Lake Pannon (e.g., Kázmér, 1990; Magyar et al., 1999; Harzhauser and Mandic, 2008; Kováč et al., 2017). The

long-living lake was gradually filled by sediments supplied from the uplifting Alps and Carpathians during the period of ~10.5–4 Ma (Magyar et al., 2013).

The succession analyzed for authigenic $^{10}Be/^{9}Be$ in the Kolárovo-4 well falls into the Vráble and Ivanka Formations. (Fig. 1C). The first one was deposited in the late Middle Miocene, the Sarmatian Central Paratethys stage constrained to ~12.6–11.6 Ma (Keith et al., 1989; Kováč et al., 2018a). However, the biostratigraphic analyses performed in the neighboring wells Modrany-1 and 2, and Nová Vieska-1 (Fig. 1B) indicated that the upper portion of this progressively deepening basin floor marine succession is missing and that only sediments of the time interval ~12.6–12.1 Ma are preserved (Kováč et al., 2018b; Vlček et al., 2020b).

The Ivanka Fm. was deposited on a lake floor by suspension settling and sediment gravity flows sourced from the shelf slope of the paleo-Danube system in between ~10.0–9.3 Ma (Fig. 1C) according to integration of biostratigraphic, magnetostratigraphic and authigenic $^{10}Be/^{9}Be$ data from this part of the basin (Magyar et al., 2007; 2013; Sztanó et al., 2016a; Šujan et al., 2016; Kováč et al., 2018b; Vlček et al., 2024). The period of 11.6–10.0 Ma is characterized by low sediment supply with deposition of just a few tens of meters of sediment, which is not included in the core samples. The paleo-Danube feeder system reached the Danube Basin only after ~10 Ma (Magyar et al., 2013; Šujan et al., 2021a; Vlček et al., 2024), thus the formation of turbidite systems occurred later. The basin floor attained water depths of up to 500 m in the Danube Basin (Balázs et al., 2018), allowing formation of thick turbiditic sequence in front of the prograding shelf slope system (sensu Johannessen and Steel, 2005; Sztanó et al., 2013; Patruno and Helland-Hansen, 2018).

The regression of Lake Pannon after ~8.9 Ma is marked by the deposition of the deltaic Beladice Fm., which reach a thickness of ca. 200–500 m in the study area and is characteristic by its predominantly sandy composition of deltaic parasequences, in contrast with the below-lying muddy shelf slope succession. It is overlain by alluvial Volkovce Fm. accumulated after ~8.6

Ma, with a predominance of overbank deposition and lower proportion of sandy channel belts (Sztanó et al., 2016a; Šujan et al., 2020; Vlček et al., 2024).

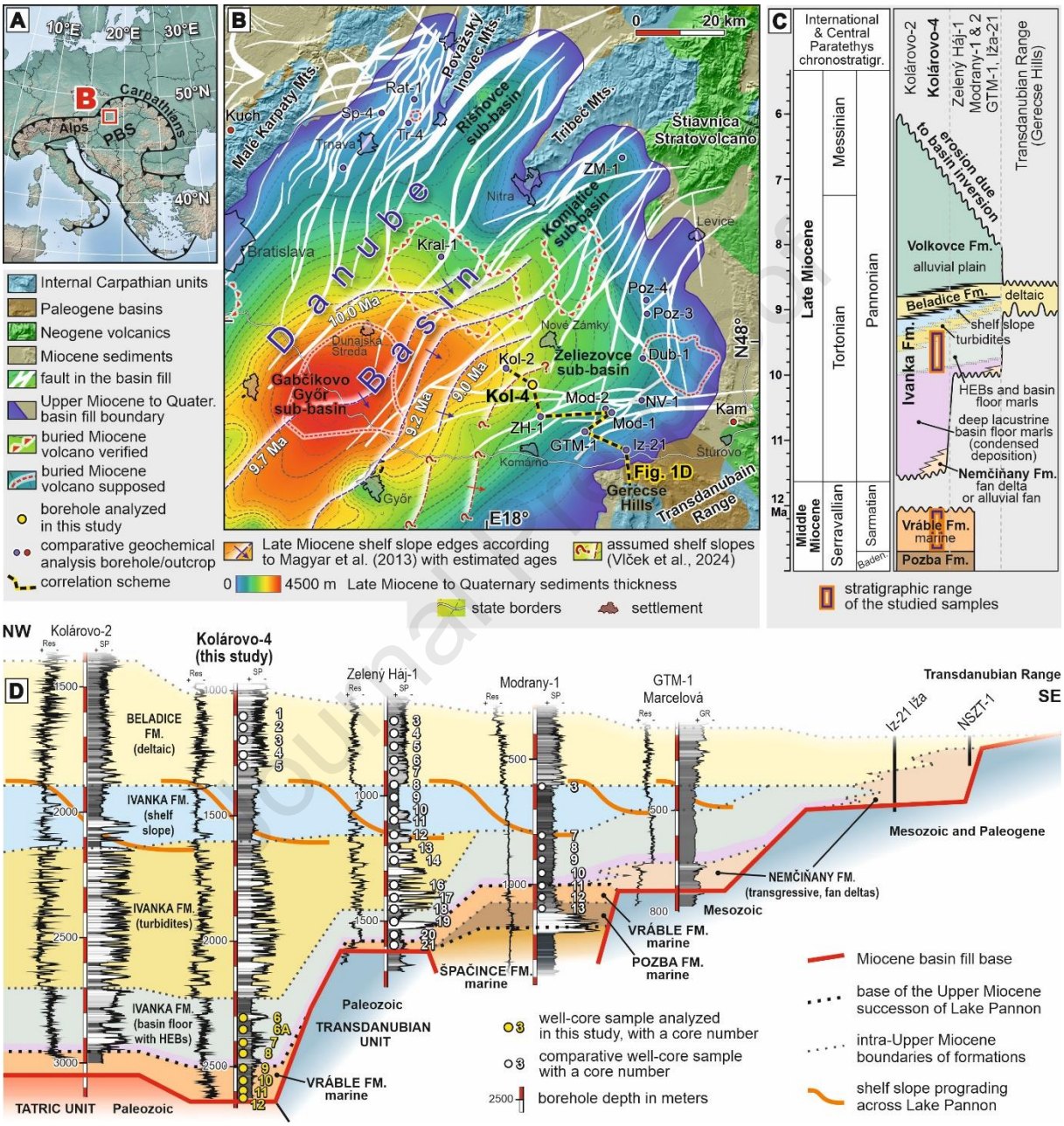


**Fig. 1.** Location and stratigraphy of the study area. **A:** Location of the study area within the Pannonian Basin System (PBS). **B:** The studied Kolárovo-4 well present on the eastern flank of the Danube Basin, together with wells and outcrops involved in the comparative geochemical analysis of provenance. Thickness map modified from Sztanó et al. (2016a).

Fault network from Šujan et al. (2025). Boundaries of stratovolcanoes buried below the basin fill according to Rybár and Kotulová (2023) and Rybár et al. (2024). **C:** Lithostratigraphy of the study area according to Sztanó et al. (2016a) and Šujan et al. (2021b). **D:** Correlation scheme showing the basin fill geometry, modified from Sztanó et al. (2016a) and Vlček et al. (2024). The correlation is flattened on the top horizon of the shelf slope succession which prograded rapidly in the studied time slice and thus represents a rough paleohorizontal indicator. Therefore, the location of well-tops does not represent recent topography. The results for the samples analyzed in other studies could be found in Kováč et al. (2018b) and Vlček et al. (2020b). Well/outcrop abbreviations in B: Dub-1, Dubník-1; GTM-1, Marcelová-1; Kam, Kamenica nad Hronom; Kral-1, Králová-1; Kuch, Kuchyňa; Mad-3, Modrany-1; Mo-2, Modrany-2; NV-1, Nová Vieska-1; Poz-3, Pozba-3; Poz-4, Pozba-4; Rat-1, Ratkovce-1; Sp-4, Špačince-4; Tr-4, Trakovice, 4; ZH-1, Zelený Háj-1; ZM-1, Zlaté Moravce-1.

# 3. Material and methods

## 3.1 Sampling strategy

The borehole cores from Kolárovo-2 and 4 well assigned to the Ivanka Fm. were suggested to include hybrid event beds (Sztanó et al., 2016b; Vlček et al., 2024). Hence, the mud included in the strata might be derived from various original sources, for example intraclasts of shelf slope muds of gravity flow origin, basin floor hemipelagic strata, muds accumulated by contour bottom currents or any type of extraclast mud from older sequences, exposed on the basin floor due to tectonics. The cores of Ivanka Fm. are therefore a good target for tracing the provenance of mud and its effect on the authigenic $^{10}Be/^{9}Be$ dating.

Seven samples from four cores of the Kolárovo-4 well were collected from the Upper Miocene Ivanka Fm.: one sample each from Core 6 and Core 6A, respectively, two samples from the core 7 and three samples taken from core 8 (Fig. 1D, Table 1). Another eight samples were

taken from the late Middle Miocene Vráble Fm., as a control on beryllium isotope inventory from a potential source of mud redeposition, taking two samples from each of the four cores 9–12 of the Kolárovo-4 well. The sampling strategy reflects the availability of muddy material in the cores. All methods involved in the study were applied to every mentioned sample, except for the organic geochemistry analysis. All samples are lithified to mudstones, sandstones, and conglomerates. As the study focuses on primary paleoenvironmental properties, the sample grain size is further discussed as mud, sand, and gravel.

### 3.2 Authigenic $^{10}Be/^{9}Be$ analysis

All samples were processed in the laboratory of Department of Geology and Paleontology, Faculty of Natural Sciences, Comenius University Bratislava (Slovakia) using a workflow described in detail in Šujan et al. (2024). It is based on the laboratory procedures developed by Bourlès et al. (1989) and Carcaillet et al. (2004), which aims to extract the authigenic Fe and Mn oxyhydroxide phase without dissolving the clastic mineral fraction, mostly composed of silicates. The samples were dried, powdered, the authigenic phase was extracted from ~2.25 g of a sample using a solution of 0.04 M $NH_2OH$–HCl in 25% acetic acid. A 2 ml aliquot of the leaching solution underwent $^{9}Be$ measurements using Plasma-Quant ICP-MS System (Analytik Jena AG) at the Institute of Chemistry, Slovak Academy of Sciences (Bratislava), employing linear regression to mitigate the matrix effect (Tan and Horlick, 1987). All beryllium concentrations fall after dilution within the standard levels of ICP-MS measurement range attaining good precision in the analytical uncertainty levels of 2–3%. The remaining fraction of the solution was spiked with 0.45 g of the Scharlau ICP-MS commercial beryllium standard solution (1000 ppm concentration), having the $^{10}Be/^{9}Be$ ratio of $7.80 \times 10^{-15}$ (Merchel et al., 2021). The solution was evaporated, and the precipitate dissolved in HCl underwent resin chemistry using cation exchange with Dowex 1x8 and anion exchange with Dowex 50wx8 (both 100–200 mesh) to separate beryllium from other elements. Samples were subjected to

196 ageing during cleaning to remove $NH_4Cl$ (Merchel et al., 2019) before being oxidized in an
197 oven under 800°C for one hour. The resulting BeO was mixed with niobium powder, pressed
198 into copper cathodes and $^{10}Be/^{9}Be$ isotopic measurements were performed AMS ASTER at
199 CEREGE, Aix-en-Provence (France). The measurements were calibrated directly against the
200 STD11 in-house standard ($^{10}Be/^{9}Be$ value of 1.191 ± 0.013 ($\times 10^{-11}$)) (Braucher et al., 2015).
201 Analytical uncertainties (reported as 1σ) include uncertainties associated with AMS counting
202 statistics, two chemical blanks measurements and the AMS internal error (0.5%). Calculated
203 ages include also the uncertainty associated with the initial ratio.

204 ## 3.3 Methods used to trace redeposition

205 ### 3.3.1 Sedimentology

206 Facies analysis of the cores cut parallel with the core axis was done by Vlček et al. (2024) and
207 the results are utilized here. It followed analysis of grain size and internal stratal geometry
208 according to Stow (2005). A special emphasis was put on the presence of "dirty sand", which
209 is attributed to changing rheology of gravity flows and formation of hybrid event beds (Baas et
210 al., 2009; 2019; Sumner et al., 2009; Zima et al., 2019).

211 ### 3.3.2 Biostratigraphy of nannoplankton and foraminifers

212 Calcareous nannofossil smear slides were prepared by the standard method of decantation
213 (Bown and Young, 1998). Nannofossils were counted in 300 fields of view using the Olympus
214 BX 50 at 1250 × magnification and oil immersion.

215 Foraminifera separation and detailed taphonomic analysis follow methods sensu Ruman et al.
216 (2021) and Holcová (1999). Systematic identification and taxonomy follow Cicha et al. (1998)
217 and Hayward et al. (2023). Documentation of main identified taxa and their preservation was
218 done using an electron scanning microscope QUANTA FEG 250.

219 The documented fossil assemblage was compared with observations made across the Danube
220 Basin in the studies by Rybár et al. (2015; 2016; 2024), Kováč et al. (2018b), Hudáčková et al.
221 (2018a; 2020), Šarinová et al. (2018; 2021b; 2021a).

222 **3.3.3 Inorganic geochemistry**

223 The comparative provenance analysis is based on the extensive measurement dataset of well
224 cores, and the values of studied proxies are included in the Supplementary Table S3. The
225 comparativeness of the whole dataset is established by analyzing all samples in the Bureau
226 Veritas mineral laboratories with the same methodology of ICP-ES (major oxides) and ICP-MS
227 (trace elements). Specific analytical procedures are described in the publication listed below.
228 Location of the sampled sites is included in Fig. 1B. The studied dataset originates from the
229 Danube Basin, which includes 15 samples of the Kolárovo-4 well analyzed in this study, and
230 additional 8 samples taken from the highstand regressive deltaic Beladice Fm. of the Kolárovo-
231 4 well (Vlček et al., 2024). Another 31 samples originate from the Zelený Háj-1 well (Vlček et
232 al., 2024), 31 samples from Modrany-1 and 19 samples from the Modrany-2 well (Vlček et al.,
233 2020a, b), 7 samples from the Pozba-4 well (Vlček et al., 2022) and 14 samples from the
234 Ratkovce-1 well (Supplementary Table S3). These samples could be classified as Langhian
235 (lower Badenian) Špačince Fm. (20 samples), Serravallian (upper Badenian and Sarmatian)
236 Pozba and Vráble fms. (34 samples), Upper Miocene (Pannonian) Ivanka Fm. (55 samples) and
237 Beladice Fm. (13 samples).

238 For tracking of re-working and/or change of provenance, the whole-rock geochemistry was
239 focused on several selected elements (Supplementary Table S3). The source area of the Danube
240 Basin sediments dominantly consists of carbonate rocks, granitoids, mica-schist, gneiss, and
241 products of Neogene volcanism. The presence of carbonates in the source rocks could be
242 tracked by Mg concentration since dolomite is less soluble in fresh water (Amorosi et al., 2020).
243 The Zr/Sc versus Th/Sc ratios were used for tracking of reworking and compositional variability

(McLennan et al., 1993), where Zr represents zircon, Th is incompatible element in igneous rocks (enriched in granites and rhyolites) and Sc represent normalization as compatible element. The Hf is also present in zircon, what is documented by their correlation. The relationships between the "immobile" elements Zr, Cr, Hf, Th, rare earth elements (REE), and also the above-mentioned Mg reflecting the source rocks were evaluated and displayed in ternary diagrams Lu-Th-Hf , Th-Ti-Zr (Riboulleau et al., 2014) and Mg-Cr-(Zr+Hf). Since the Middle Miocene evolution of the Danube Basin was dominated by volcanism, the whole rock analyses of volcanic and pyroclastic samples from the Danube Basin and nearby areas were use for comparison (Kováč et al., 2018b; Šarinová et al., 2018; 2021a; Rybár et al., 2019; 2024).

The analysis is complicated by various factors. The carbonate content "dilutes" the concentrations of elements from terrigenous sources. The carbonate content was calculated from inorganic C (Supplementary Table S3). Another factor is variation of sediment grain size of the compared samples. This can be inferred from the $SiO_2/Al_2O_3$ ratio, where a higher $SiO_2/Al_2O_3$ ratio indicates a higher proportion of sand sized grains. To minimize these problems, the enrichment factor relative to the UCC (Upper Continental Crust; McLennan, 2001) was calculated for Mg, Th, Cr, Zr and Hf using the formula:

$$X_{EF} = (X_{sample}/Al_{sample}) / (X_{UCC}/Al_{UCC})$$

### 3.3.4 Organic geochemistry

Six mudstone samples were processed for biomarker analysis, three from each of the Ivanka and Vráble fms. (Supplementary Table S4). Biomarkers were extracted from powdered rock using a dichloromethane (DCM) and methanol mixture (93:7) with a Dionex ASE 100 system. Saturated hydrocarbon fractions (SAT) were separated on a silica column using n-hexane and DCM. The SAT fraction was analyzed via gas chromatography-mass spectrometry (GC-MS) using an Agilent A6890N chromatograph and an Agilent 5973N quadrupole mass spectrometer,

with helium as the carrier gas. A DB-1MS (60 m/0.250 mm/0.25 µm) OV1 column and a temperature program of 50°C (2 min), 2°C/min to 310°C (20 min), at a flow rate of 1.3 ml/min, were used. Mass chromatograms for m/z 57 (n-alkanes) were evaluated with Agilent MassHunter software. The results gained from the six samples originating from the Kolárovo-4 well were compared to the values obtained from the nearby Zelený Háj-1 well with much lower proportion of hybrid event beds (Vlček et al., 2024).

In organic geochemistry, the abundance of n-alkanes provides insights into supply of terrestrial material to marine environment. Generally, a predominance of long-chain homologues (n-$C_{27}$ to n-$C_{33}$) is attributed to terrestrial land plant inputs (Cranwell, 1973), while mid-chain homologues (n-$C_{21}$ to n-$C_{25}$) indicate the presence of macrophytes (submerged, emergent, and floating plants; Ficken et al., 2000), and short-chain homologues (n-$C_{15}$ to n-$C_{20}$) mainly originate from microbial biomass and various degradation processes (e.g., Gocke et al., 2013). The carbon preference index (CPI) is used to indicate the degree of diagenesis of straight-chain geolipids; it is a numerical representation of how much of the original biological chain-length specificity is preserved in geological lipids (Meyers and Ishiwatari, 1993). Biomarkers from different biological origins have different CPI values. For instance, n-alkanes from the cuticular waxes of higher plants have a strong odd/even predominance and give high CPI values (> 5), CPI values around 1 are characteristic for highly degraded OM and/or presence of large amounts of microorganism derived OM (Cranwell et al., 1987). The CPI values of n-alkanes can indicate the maturity of organic matter. Hence, a comparison of biomarker inventory of formations, deposited in contrasting environments and having different biological origins of biomarkers, can provide an insight into redeposition of sediment, especially fine grained, which preferably bounds the organic matter. The ACL of alkanes is used to differentiate between predominantly terrestrial OM and degraded OM or microorganism occurrence. ACL ≥ 25 is considered indicative of organic matter (OM) derived from higher plants (long-chain alkanes),

while ACL ≤ 25 indicates degraded OM or microorganism derived from OM (short-chains alkanes) (Bray and Evans, 1961; Gocke et al., 2013; Salocchi et al., 2021). The TAR index (terrigenous/aquatic ratio; Bourbonniere and Meyers 1996) quantifies the *in situ* algal vs. terrestrial organic matter, where TAR values greater than 1 indicate organic matter derived from terrestrial plants, whereas values below 1 suggest sources from marine or freshwater algae.

# 4. Results

## 4.1 Authigenic $^{10}Be/^{9}Be$ record

Table 1 and Fig. 2 show the values of measured isotopic ratio in analyzed 15 samples, together with corresponding ages calculated based on lacustrine initial ratio of $6.99 \pm 0.14 \times 10^{-9}$ from Šujan et al. (2016). Despite relatively low AMS $^{10}Be/^{9}Be$ ratios in the order of $10^{-14}$, relatively stable currents resulted in AMS uncertainties of 3.0–7.3%. All measured AMS $^{10}Be/^{9}Be$ ratios reached values higher than the processing blanks, which represent the detection limit, despite some samples yielded very close values. The natural authigenic $^{10}Be/^{9}Be$ ratios of the Middle Miocene Vráble Fm. exhibit low variability from $4.4 \pm 0.3 \times 10^{-12}$ to $9.0 \pm 0.4 \times 10^{-12}$, yielding authigenic $^{10}Be/^{9}Be$ ages from 13.1 ± 0.6 Ma to 14.7 ± 0.9 Ma. A trend of increase in isotopic ratio and a decrease in age upwards could be seen, despite the ages overlap within the uncertainty. This range does not overlap with the interval ~12.6–12.1 Ma, independently determined by biostratigraphy of the associated Sarmatian fossils (Kováč et al., 2018b; Vlček et al., 2020b).

The natural authigenic $^{10}Be/^{9}Be$ ratios from the Upper Miocene Ivanka Fm. show significantly higher variability and scatter, ranging from $8.6 \pm 0.4 \times 10^{-12}$ to $66.8 \pm 2.5 \times 10^{-12}$. Despite the higher variability, a trend of increase in isotopic ratios upwards can be seen, except for the sample Kol-4-7b. This trend is reflected in the decrease of calculated ages upwards from 13.4 ± 0.6 Ma to 11.2 ± 0.4 Ma, after excluding the age 9.3 ± 0.4 of the sample Kol-4-7b. Again,

317 this age interval does not overlap with the independently determined age of ~10.0–9.3 Ma for
318 this succession (Sztanó et al., 2016a; Vlček et al., 2024).

319

Journal Pre-proof

**Table 1:** Concentrations of $^{9}Be$ and $^{10}Be$, $^{10}Be/^{9}Be$ ratios and calculated ages for the analyzed samples. Uncertainties are 1σ. Concentrations of $^{10}Be$ are corrected for the $^{10}Be/^{9}Be$ ratio of three processing blanks with the values between $7.64 \times 10^{-15}$ and $8.53 \times 10^{-15}$. The sample ID includes well name abbreviation (Kol-4) and the number of core (e.g., "6" in Kol-4-6a). In the case of collecting several samples from single core, lowercase letters distinguish the samples (e.g., "a" in Kol-4-7a). * - sample diverging from the general observed trend. The approach of the "Sarmatian" initial ratio, which reaches $2.64 \pm 0.25 \times 10^{-9}$, is explained in the discussion chapter.

| Sample ID | Depth of the well-core (m) | Lithostrati-graphy | $^{9}Be$ (at × $g^{-1}$) × $10^{16}$ | AMS $^{10}Be/^{9}Be$ (× $10^{-14}$) | $^{10}Be$ (at × $g^{-1}$) × $10^{5}$ | Natural $^{10}Be/^{9}Be$ (× $10^{-12}$) | Age based on lacustrine initial ratio (Ma) | Initial $^{10}Be/^{9}Be$ for the age 12.6–12.1 Ma (× $10^{-9}$) | Age based on the "Sarmatian" initial ratio (Ma) |
|---|---|---|---|---|---|---|---|---|---|
| Kol-4-6a | 2306 | Ivanka Fm. | 6.294 ± 0.189 | 6.306 ± 0.196 | 16.617 ± 0.516 | 26.400 ± 0.975 | 11.163 ± 0.431 | | 9.215 ± 1.049 |
| Kol-4-6b | 2353 | Ivanka Fm. | 1.348 ± 0.040 | 1.461 ± 0.081 | 1.983 ± 0.110 | 14.704 ± 0.869 | 12.335 ± 0.709 | | 10.386 ± 1.280 |
| Kol-4-7a | 2405 | Ivanka Fm. | 10.262 ± 0.308 | 3.794 ± 0.127 | 9.199 ± 0.307 | 8.964 ± 0.349 | 13.325 ± 0.545 | | 11.376 ± 1.282 |
| Kol-4-7b* | 2408 | Ivanka Fm. | 6.315 ± 0.189 | 14.674 ± 0.463 | 42.200 ± 1.330 | 66.825 ± 2.495 | 9.305 ± 0.355 | n.a. | 7.357 ± 0.857 |
| Kol-4-8a | 2448 | Ivanka Fm. | 9.743 ± 0.292 | 3.600 ± 0.128 | 8.644 ± 0.306 | 8.872 ± 0.361 | 13.345 ± 0.565 | | 11.397 ± 1.292 |
| Kol-4-8b | 2450 | Ivanka Fm. | 3.848 ± 0.115 | 2.687 ± 0.101 | 5.796 ± 0.218 | 15.063 ± 0.641 | 12.286 ± 0.535 | | 10.338 ± 1.189 |
| Kol-4-8c | 2451 | Ivanka Fm. | 9.837 ± 0.295 | 3.517 ± 0.133 | 8.459 ± 0.319 | 8.599 ± 0.367 | 13.408 ± 0.590 | | 11.460 ± 1.308 |
| Kol-4-9a | 2507 | Vráble Fm. | 3.506 ± 0.105 | 1.458 ± 0.108 | 2.144 ± 0.158 | 6.113 ± 0.467 | 14.091 ± 1.035 | 2.931 ± 0.367 | |
| Kol-4-9b | 2509 | Vráble Fm. | 5.130 ± 0.154 | 1.947 ± 0.130 | 3.615 ± 0.241 | 7.046 ± 0.490 | 13.807 ± 0.928 | 3.378 ± 0.423 | |
| Kol-4-10a | 2556 | Vráble Fm. | 5.785 ± 0.174 | 2.630 ± 0.097 | 5.716 ± 0.211 | 9.880 ± 0.415 | 13.130 ± 0.569 | 4.736 ± 0.593 | |
| Kol-4-10b | 2559 | Vráble Fm. | 4.117 ± 0.123 | 1.703 ± 0.085 | 2.843 ± 0.141 | 6.907 ± 0.370 | 13.846 ± 0.738 | 3.311 ± 0.415 | |
| Kol-4-11a | 2596 | Vráble Fm. | 3.844 ± 0.115 | 1.329 ± 0.077 | 1.706 ± 0.098 | 4.439 ± 0.271 | 14.731 ± 0.883 | 2.128 ± 0.267 | n.a. |
| Kol-4-11b | 2598 | Vráble Fm. | 3.307 ± 0.099 | 1.521 ± 0.081 | 2.340 ± 0.125 | 7.076 ± 0.405 | 13.798 ± 0.778 | 3.392 ± 0.425 | |
| Kol-4-12a | 2625 | Vráble Fm. | 1.238 ± 0.037 | 0.984 ± 0.062 | 0.670 ± 0.042 | 5.417 ± 0.357 | 14.333 ± 0.920 | 2.597 ± 0.325 | |
| Kol-4-12b | 2627 | Vráble Fm. | 3.786 ± 0.114 | 1.315 ± 0.067 | 1.700 ± 0.087 | 4.490 ± 0.247 | 14.708 ± 0.805 | 2.152 ± 0.270 | |

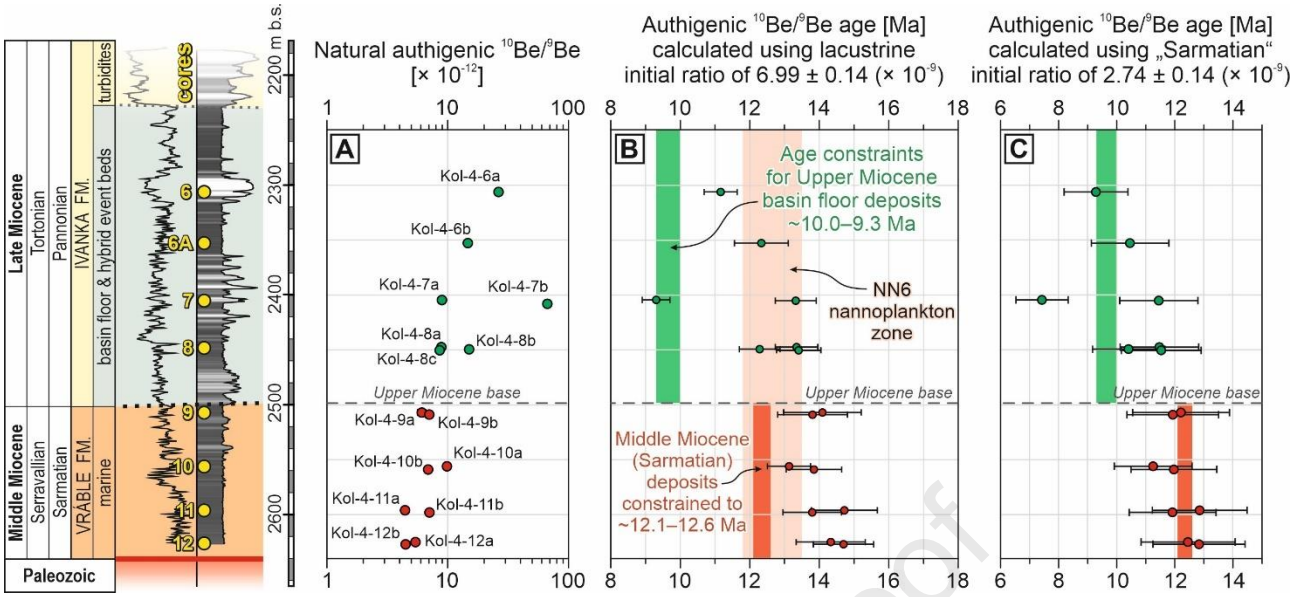


**Fig. 2.** Distribution of the analyzed samples along the profile of the Kolárovo-4 well. (A) Natural authigenic $^{10}Be/^{9}Be$ ratios. Error bars for the natural authigenic $^{10}Be/^{9}Be$ ratios are smaller than the sample symbol. Note the logarithmic scale. (B) Authigenic $^{10}Be/^{9}Be$ ages calculated using the lacustrine initial ratio of 6.99 ± 0.14 × $10^{-9}$ from Šujan et al. (2016) and (C) using the "Sarmatian" initial ratio obtained by back-calculation based on the samples from the Middle Miocene Vráble Fm. with a value of 2.67 ± 0.14 × $10^{-9}$. See discussion for explanation of the back-calculation.

## 4.2 Evidence for mud redeposition in the Upper Miocene basin floor Ivanka Fm. and its potential sources

### 4.2.1 Sedimentology

As described and discussed in Vlček et al. (2024), the basin floor interval of the Ivanka Fm. analyzed in this study consists of a relatively high proportion of sandy beds, which are either massive, with faint lamination or well-developed lamination, which is commonly convex as well as concave (Fig. 3). Flame structures indicating rapid deposition and soft-sediment deformation are ubiquitous, as well as mud intraclasts. The bed geometries and grain size distribution imply a deposition of sand from suspension by laminar high sediment-concentrated flows and by supercritical high-density flows (Baas et al., 2009; Kane and Ponten, 2012; Talling et al., 2012). Moreover, a significant proportion

344 of sandy beds bear characteristics of "dirty sand" with high admixture of mud, which together with
345 internal deformations and the presence of mud intraclasts indicate a deposition of hybrid event beds
346 (Haughton et al., 2009; Kane and Ponten, 2012; Fonnesu et al., 2018).

347

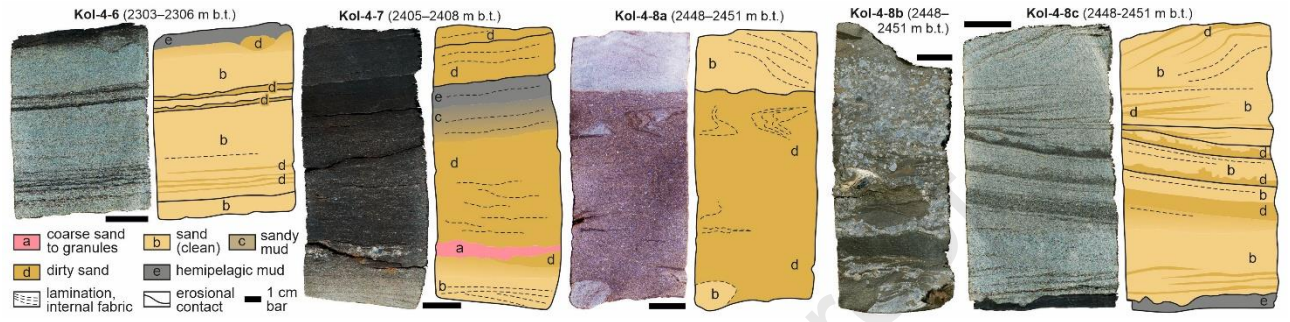


348

349 **Fig. 3.** Examples of well cores from the basin flood interval of the Ivanka Fm. in the Kolárovo-
350 4 borehole (modified from Vlček et al., 2024). Note the overall sandy nature and ubiquitous
351 presence of "dirty sand", implying deposition of hybrid event beds.

352 **4.2.2 Biostratigraphy**

353 For biostratigraphy, the calcareous nannofossils and foraminifera were studied. The assemblage
354 documented by the calcareous nannoplankton analysis from six cores of the Kolárovo-4
355 (Supplementary Table S1) is assigned to the Sarmatian – correlated to the NN6 and ?Pannonian
356 ranked accordingly based on the presence of ?*Isolithus semenenkoii* and *?Noelaerhabdus bozinovicae*
357 (Galović, 2020; Ćorić, 2021; Ćorić et al., 2023). The Sarmatian assemblage includes *Calcidiscus*
358 *macintyrei, Coccolithus miopelagicus, Helicosphaera walbersdorfensis, Orthorhabdus rugosus, O.*
359 *serratus, Reticulofenestra pseudoumbilicus, R. producta, Sphenolithus abies* and *Syracosphaera*
360 *pulchra* (Supplementary Table S1). The samples ranging from Kol-4-7a to Kol-4-9b contain fossils
361 supporting the possible Pannonian age or Sarmatian interval of the NN6 Zone. The lowermost
362 samples, Kol-4-10b and Kol-4-11b, are assigned to the NN6 Zone. An abundant reworking primarily
363 of the Middle Miocene, but including the Lower Miocene, Paleogene, and Cretaceous fossils is also
364 present, making distinguishing of autochthonous assemblage challenging.

Foraminifera show a similar situation (Supplementary Table S2), as the samples from cores 4 to 7 contain scarce fine agglutinated species of *Miliammina* and *Lagenammina* genera (Fig. 4), which are often considered as the indicators of the Pannonian age (Late Miocene) in the Vienna and Danube basins (Fuchs and Schreiber, 1988; Hudáčková et al., 2018b). The sample Kol-4-8b yields frequent pyrite tubes, high abundance of which is characteristic for the base of the Pannonian succession in the Vienna Basin (Harzhauser et al., 2018; Lin et al., 2023). The tubular pyrite aggregates, together with the presence of very poorly preserved and rare Sarmatian specimens from *Nonion* and *Elphid* genera (Fig. 4) can document the earliest Pannonian age. The cores 9, 10, 11, and 12 of the Kolárovo-4 well contain an assemblage dominated by *Elphidium hauerinum, E. excavatum, E. macellum, Anoimalinoides* cf. *dividens, Nubecularia* sp. of *Elphidium hauerinum* Zone (Sarmatian; Grill, 1941) (Fig. 4, Supplementary Table S2). Samples from the upper cores 6 and 7 contain foraminifera tests and inner casts, reworked from the Badenian (*Globigerina* sp. cf. *bulloides*, *Bolivina* sp., Cibicides sp.) and Sarmatian successions (*Nonion*, *Porosonion*, *Elphidium*, Fig. 4). Beside the mentioned fossils, the cores 6 and 7 contain also fish scales, coalified glyptostrobe conus seeds and Porifera spicules.

Journal Pre-proof

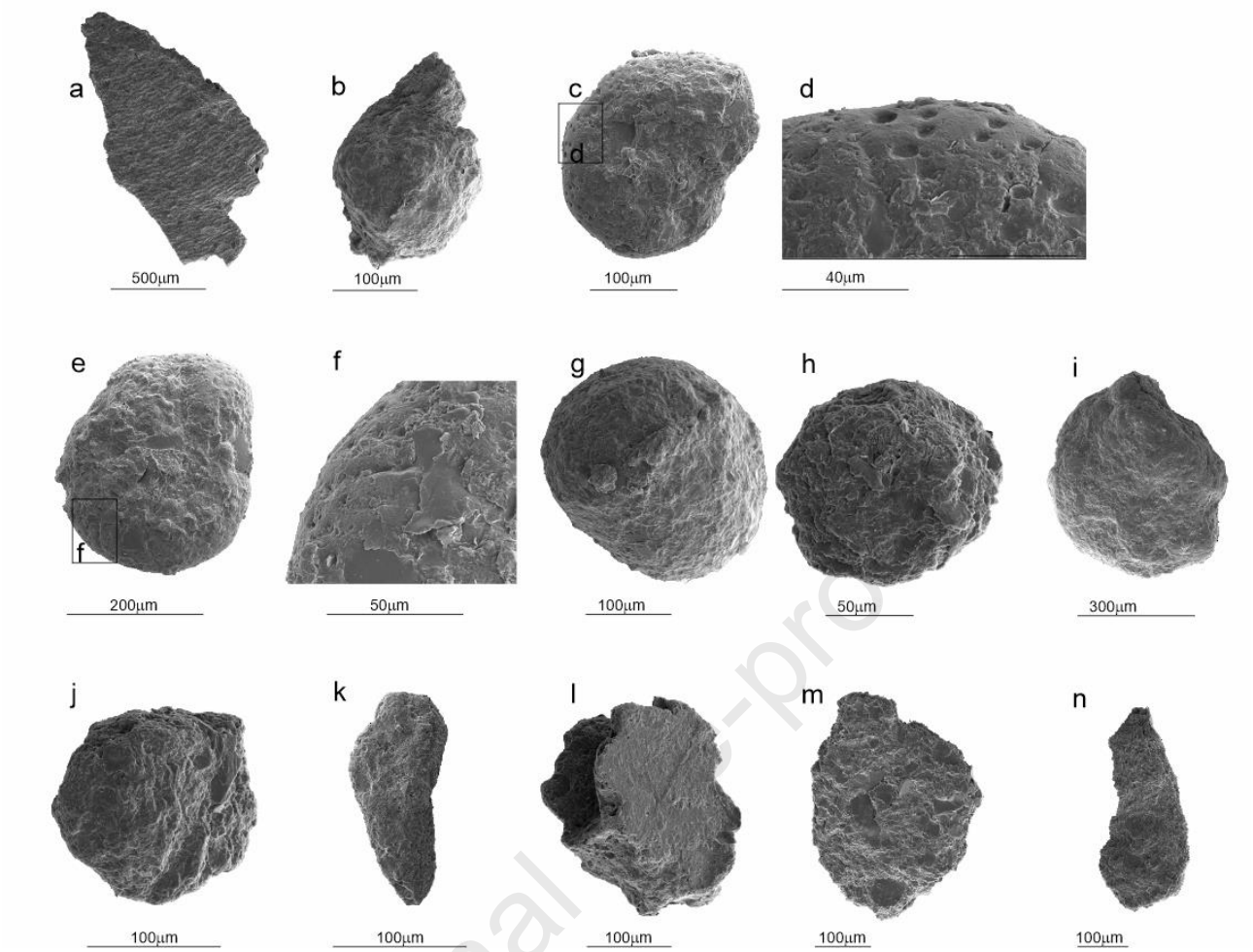


**Fig. 4.** Fossil remains identified during investigation of the foraminiferal assemblage of the basin floor interval of the Ivanka Fm in the Kolárovo-4 well, except for (I) and (N) from the uppermost Vráble Fm. (A) Fragment of the fish scale, sample Kol-4-7b. (B) Cast of *Globigerina* sp. indet, sample Kol-4-7b. (C) *Porosononion* sp. cf. *P. granosum* (d'Orbigny, 1846), sample Kol-4-8a. (D) Detail of the wall pores of the *Porosononion* sp. cf. *P. granosum* (d'Orbigny, 1846) with signs of dissolving, sample Kol-4-8a. (E) *Porosononion* sp. cf. *P. granosum* (d'Orbigny, 1846) with signs of dissolving (d'Orbigny, 1846), sample Kol-4-8b. (F) Detail of the wall pores of the *Porosononion* sp. cf. *P. granosum* (d'Orbigny, 1846) with signs of dissolving, sample Kol-4-8b. (G) ? *Porifera rhaxi*, sample Kol-4-6b. (H). Unspecified rotaliid foraminifera, sample Kol-4-7b. (I) *Elphidium* cf. *hauerinum* (d'Orbigny, 1846), sample Kol-4-9b from the Vráble Fm. (J) *Pararotalia* cf. *aculeata* (d'Orbigny, 1846), Kol-4-7b. (K) *Bolivina* sp. indet., sample Kol-4-6b.

(L) Fragment of *Lobatula lobatula*, Kol-4-7b. (M) *Miliammina* sp., Kol-4-7b. (N) *Ammobaculites* sp. indet., Kol-4-9b from the Vráble Fm.

### 4.2.3 Inorganic geochemistry

Epiclastic samples were evaluated for comparative geochemical analysis in terms of recycling and change of provenance. All samples have similar character, and their composition varies dominantly with grain-size ($SiO_2/Al_2O_3$ = 2.4–8.6) and amount of carbonate admixture ($CO_2$ = 0.2–19.9; Supplementary Table S3). Although the calculation of enrichment factors was used for minimalizing of these effect, some general trends are still present. Another problem to be considered is diagenetic and/or intraformational enrichment, specifically the extreme increase in Si content ($SiO_2/Al_2O_3$ more than 8 for single sample), likely due to biogenic production, and the diagenetic mobility of other elements (single Fe carbonate sample) (Figs. 5, 6). Biogenic Si production was documented, for example, in Fe-rich sample form the Zelený Háj-1, core 16, where diagenetic overprint caused high Fe carbonate content and REE enrichement (Figs. 5 and 6; Vlček et al. 2024). These samples are marked separately as outlier types due to their specific origin. Similarly, the sandy samples ($SiO_2/Al_2O_3$ reaching >5.5) are grouped separately, due to slightly different behavior. All sandy samples are Zr and Hf enriched, what points to cumulating of zircons in the sand fraction.

After considering these factors, the most significant change in the composition of the Danube Basin Miocene sediments is shown in the content of $Zr_{(EF)}$ and $Hf_{(EF)}$. This factor points to a zircon addition due to recycling of sediment (Figs. 5, 6). The second factor is the content of $Mg_{(UCC)}$, what reflects the proportion of dolomite. Based on these criteria, the samples were divided to four categories: type 1 represents samples with low content of $Zr_{(EF)}$ and $Hf_{(EF)}$ (lower than 0.67 and 0.65 respectivelly, Supplementary Table S3), what indicates minimal to no sediment reworking (Fig. 5). Types 2–4 are typical by higher content of $Zr_{(EF)}$ and $Hf_{(EF)}$ (more than 0.67 and 0.65 respectivelly, Supplementary Table S3), reflecting a zircon addition via sediment recycling (Fig.5; McLennan et al., 1993). This

division is supported by the distribution of andesite volcaniclastis samples from Danube Basin, whose compositional variability line divides these two major groups (Fig. 5).

The type 2–4 group can be subdivided by content of $Mg_{(EF)}$ to Mg enriched type 2 ($Mg_{(EF)}$ more than 1.8), type 3 without Mg enrichment and type 4, which grouped samples with $SiO_2/Al_2O_3$ ratio more than 5.5 (sandy samples). However, this subdivision is indistinct, since the transition between individual subtypes is smooth (Fig. 5, 6). The types 2 and 3 reflect change in provenance, where type 2 represents significant dominance of carbonates (dolomites) in the source area. Although Mg enrichment can be also caused by diagenetic dolomitization, the dominance of detrital dolomite influence is the preferred interpretation. This is supported by the presence of Mg enrichment also in sandy samples (type 4), detrital origin of some carbonate grains observed by Vlček et al. (2024), and the presence of carbonate rocks in the source area. Nevertheless, also intrabasinal carbonates containing fossil shells are present apart from the detrital carbonate admixture. It is worth mentioning that type 2 samples are present mainly in the wells situated close to areas with pre-Cenozoic carbonate rocks, present also in the basin basement. A gradual change from type 2 to type 3 upward can be observed in these wells (Supplementary Table S3). Kolárovo-4 well shows a different pattern with an opposite change in provenance from type 3 in Serravallian to type 2 during Pannonian (Ivanka and Beladice fms.). Thich change in provenance is also supported by the presence of volcanic clasts in the Serravallian sediments in Kolárovo-4 well (Vlček et al., 2024).

Comparison of nonvolcanic and volcanic/pyroclastic sediments of the Danube Basin show different trends between these sediments. Whereas compositional variability of volcaniclastics/pyroclastics mirrors magma evolution, the nonvolcanic sediments reflect sediment recycling (Fig. 5). Additionally, it points to the overall intermediate character of source rocks for nonvolcanic sediments. The interlayering volcanic/pyroclastic and volcanic sediments is typical for the Middle Miocene Danube Basin fill (Šujan et al., 2025) (Fig. 5, 6). Nevertheless, the sediments of volcanic origin retain different characteristics in comparison to non-volcanic sediments, even though volcanic centers

441 formed a significant proportion of rocks in the source area from the end of the lower Badenian
442 (Langhian) up to present-day.

443 The Upper Miocene deltaic Beladice Fm. consists dominantly of type 1 ($Zr_{EF}$ and $Hf_{EF}$ lower than
444 0.65) and less type 2 which represented more recycled horizons with higher content of detritic
445 carbonates (Fig. 5, 6; Supplementary Table S3). Both types are present in the Kolárovo-4 and Zelený
446 Háj-1 wells in interfingering levels. The zircon addition via recycling is supported by the increased
447 $Zr_{EF}$ and $Hf_{EF}$ with $SiO_2/Al_2O_3$ ratio. The location of Zelený Háj-1 well close to the Transdanubian
448 Range basement built mainly of carbonate rocks (Fig. 1D; Budai et al., 2015) is reflected in high
449 $Mg_{EF}$, which is present also in type 1 there.

450 The Upper Miocene Ivanka Fm., which is the main focus of this study, contains all geochemical types
451 of sediments (Figs. 5, 6, Supplementary Table S3). The samples included in the type 1 generally
452 belong to the turbidite and shelf slope parts of the Ivanka Fm. (Fig. 7), while it also includes a major
453 part of the below-situated basin floor interval in the Zelený Háj-1 well and the upper third of the basin
454 floor interval in Modrany-1 well (Fig. 7). The second most often represented geochemical group,
455 characteristic by zircon addition via recycling (Fig. 6) is the type 2 (Mg-rich) and 3 (Mg-poor). The
456 types 2 and 3 appear in the basin floor interval of the Kolárovo-4 well, investigated in this study for
457 authigenic $^{10}Be/^{9}Be$, and lower 120 m of the basin floor interval in the Modrany-1 well (Fig. 7). A
458 subgroup designated as type 2 (Mg-rich) is restricted mainly to the shelf slope interval in the Zelený
459 Háj-1 well (Fig. 7, Supplementary Table S3). A minor group of samples indicated as type 4 of the
460 Ivanka Fm, interpreted as sandy size is present in the core 17 of the Zelený Háj-1 well (turbidite),
461 core 10 of the Modrany-1 well, and core 8 of the Kolárovo-4 well (basin floor interval). The sample
462 from core 6 of the Kolárovo-4 has extremelly high content Si; therefore, this sample was excluded
463 from the previously discussed types.

464 The Vráble and Pozba fms. of the Middle Miocene age (Sarmatian and late Badenian; Serravallian)
465 are represented only by a group of geochemical types 2–4 which document presence of sediment

recycling (Fig. 5, 6). The type 3 represents the stratigraphic interval underlying the Upper Miocene basin floor strata of the Ivanka Fm., including the Kolárovo-4 well samples analyzed for authigenic $^{10}Be/^{9}Be$ in this study (Fig. 7). An exception could be seen in the Modrany-1 well area, where type 2 (Mg-rich) is dominant probably in response to the carbonate source rocks present in basement of this area. The type 4 assumed as sub-group with a relatively higher content of sand, resulting in higher Zr concentrations is also rarely present.

The samples from the lower Middle Miocene (lower Badenian; Langhian) Špačince Fm. show again dominant geochemical Zircon-rich types 2–4 (Fig 6). This group of samples plots towards significant effect of sediment recycling in Fig. 5, comparable to the type 3 of the Ivanka, Vráble and Pozba fms. The Mg-rich type 2 is repeatedly typical for Modrany-1 well, whereas type 3 dominated in other wells. Sandy type 4 is also present.

The observed pattern show a stratigraphic relationship, with the first dominant geochemical type 1 characteristic by lower degree of sediment recycling being present in the Beladice Fm., as well as in the shelf slope, turbiditic and locally upper part of the basin floor interval of the Ivanka Fm. The Zr-rich types 2–4 with significantly higher degree of sediment recycling appear in the majority of the basin floor interval of the Ivanka Fm., and in all belowlying formations of the Middle Miocene age. Althrough the majority of the samples occupied shale field in the diagram of Herron (1988), the increase of Zr content with $SiO_2/Al_2O_3$ ratio can be observed (Supplementary Table S3). It indicates a switch from Zr-rich types 2–4 to Zr-poor type 1 reflecting a change in sediment routing pathways.

Journal Pre-proof

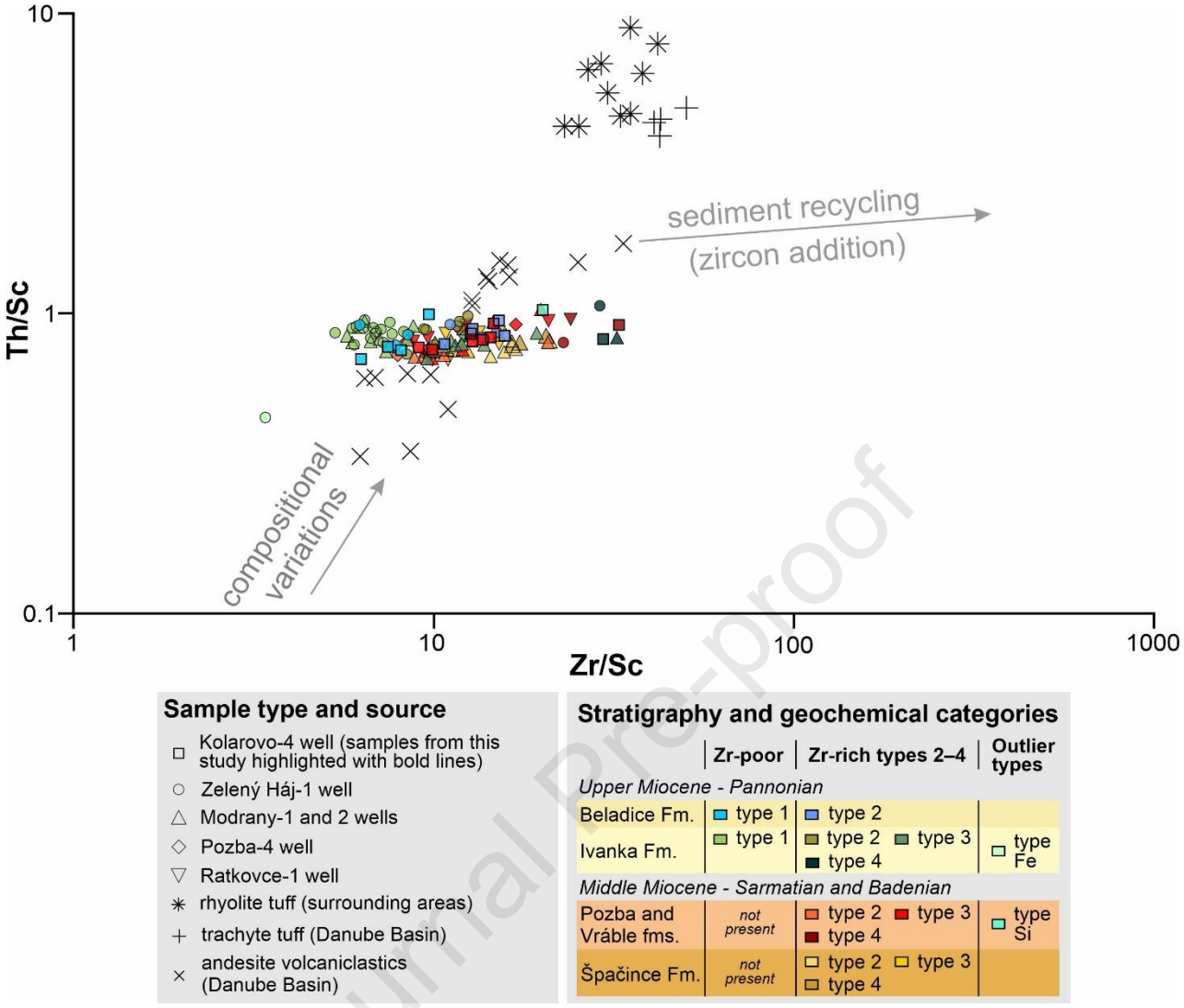


**Fig. 5.** Diagram of Th/Sc versus Zr/Sc according to McLennan et al. (1993), showing the samples included in the comparative geochemical analysis. The diagram indicates enrichment of zircon (higher Zr/Sc ratio), which is associated with sorting and recycling. The geochemical categories (types) are established according to the distribution of values observed in this study and are described in the text. The sites used for the comparative analysis are shown in Fig. 1B.

Journal Pre-proof

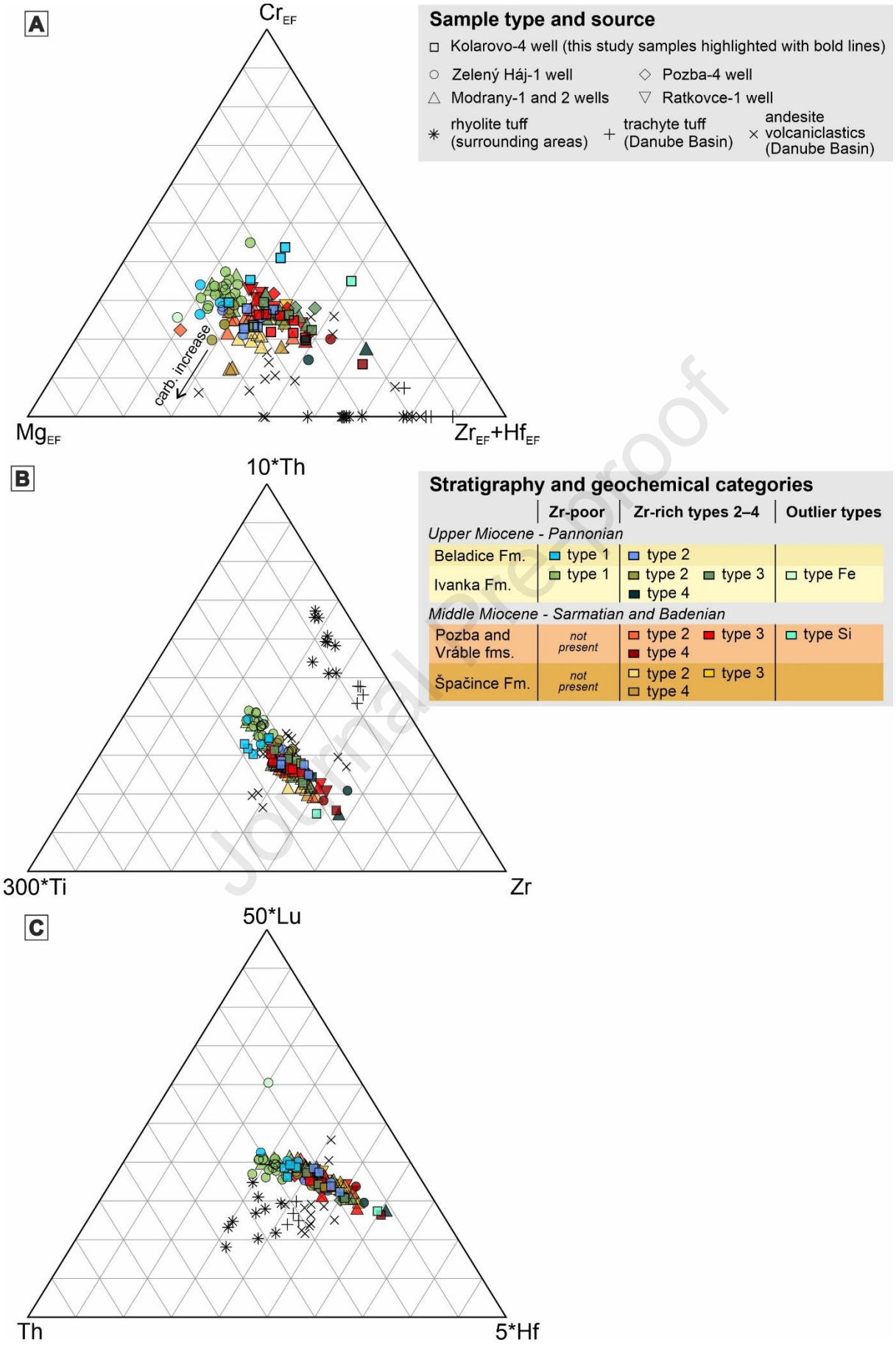
A
$Cr_{EF}$
$Mg_{EF}$
$Zr_{EF}+Hf_{EF}$
carb. increase
Sample type and source
Kolarovo-4 well (this study samples highlighted with bold lines)
Zelený Háj-1 well
Pozba-4 well
Modrany-1 and 2 wells
Ratkovce-1 well
rhyolite tuff (surrounding areas)
trachyte tuff (Danube Basin)
andesite volcaniclastics (Danube Basin)
B
10*Th
300*Ti
Zr
Stratigraphy and geochemical categories
Zr-poor
Zr-rich types 2–4
Outlier types
Upper Miocene - Pannonian
Beladice Fm.
type 1
type 2
Ivanka Fm.
type 1
type 2
type 3
type 4
type Fe
Middle Miocene - Sarmatian and Badenian
Pozba and Vráble fms.
not present
type 2
type 3
type 4
type Si
Špačince Fm.
not present
type 2
type 3
type 4
C
50*Lu
Th
5*Hf

491

**Fig. 6A.** $Mg_{EF}$-$Cr_{EF}$-$Zr_{EF}$+$Hf_{EF}$ diagram showing smooth transition between Mg-rich (type 2) and Mg-poor (type 3) samples. The two sandy samples (type 4) are Mg-rich. **B, C.** The Provenance ternary diagram (Riboulleau et al., 2014). For comparison, also samples of volcanic origin from Danube Basin and surrounding areas were displayed (Supplementary Table S3). The sites used for the comparative analysis are shown in Fig. 1B.

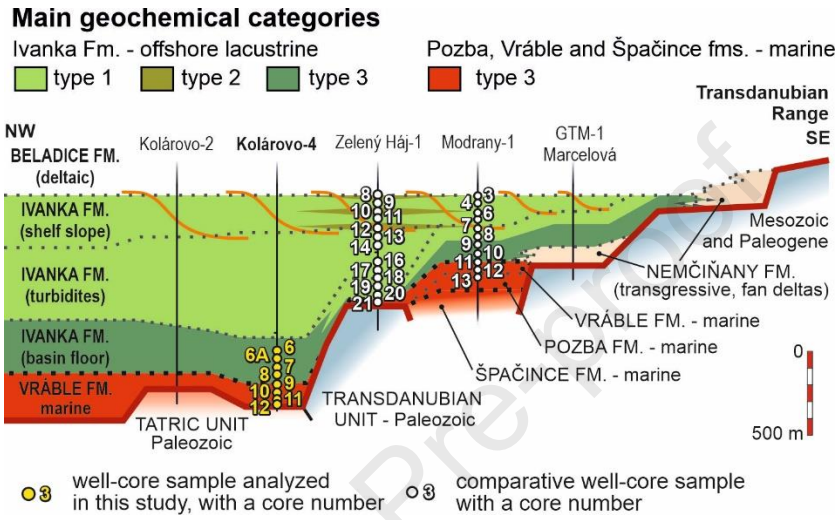


**Fig. 7.** Simplified correlation through the wells on the southeastern margin of the Danube Basin, with distribution of main geochemical types defined in this study (modified from Fig. 1D, see explanations there).

### 4.2.4 Organic geochemistry

The distribution of n-alkanes (m/z 57 ion chromatogram) is characterized by the predominance of mid-chain-length homologs in the analyzed samples from the Kolárovo-4 well. N-alkanes ranging from n-C18 to n-C23 predominate in the three samples Kol-4-6a, Kol-4-7a and Kol-4-8c from the Ivanka Fm. (Upper Miocene, Pannonian), with a maximum at n-C21 (Supplementary Table S4). On the other hand, the distribution of n-alkanes in the samples Kol-4-9b, Kol-4-10b and Kol-4-11b from the Vráble Fm. (Middle Miocene, Sarmatian) is defined by the dominance of short-chain homologs (n-C16 to n-C20), with a maximum at n-C18. However, mid- to long-chain homologs (ranging from n-C22 to n-C29) prevail in sample Kol-4-10b, with maxima at n-C26 and n-C27 (Supplementary Table S4).

Generally, higher values of long-chain n-alkanes are observed in the Sarmatian samples (25–41%) compared to the Pannonian samples (17–24%) (Fig. 8). The distribution of short-chain n-alkanes is higher in Pannonian samples (Ivanka Fm.) (37–43%) than in Sarmatian samples (26–43%), where, conversely, mid-chain n-alkanes predominate (38-40%; Fig. 8, Supplementary Table S4). The CPI values are relatively consistent across all samples from the Kolárovo-4 well, ranging between 1.16 and 1.59 and indicating highly degraded OM and/or presence of large amounts of microorganism derived OM (Fig. 8). All Kolárovo-4 samples have TAR values lower than 1, indicating the presence of aquatic OM. However, in sample Kol-4-10b, the TAR values increase, reaching up to 1.80, which indicates terrestrial OM. ACL21-35 values range between 24.65 and 26.78. Lower ACL values in the Pannonian samples (Ivanka Fm.) may indicate more degraded organic matter compared to the Sarmatian samples (Vráble Fm.).

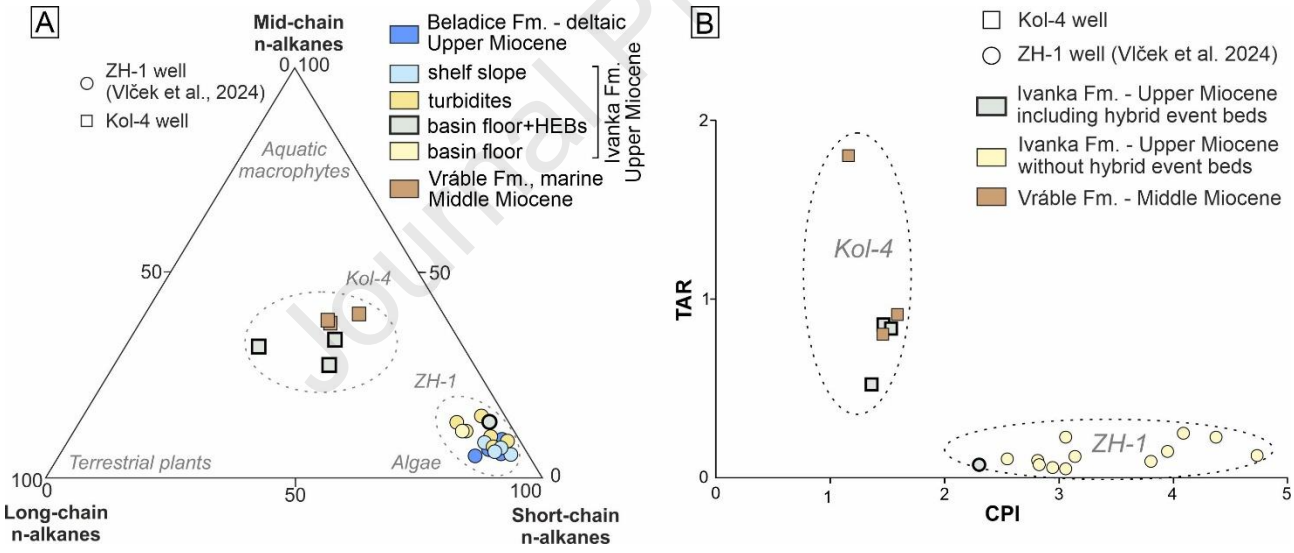


**Fig. 8.** Diagrams with selected organic geochemistry parameters. **A.** Distribution of short (n-C12–20), mid (n-C21–25) and long (n-C27–33) chain n-alkanes in the different facies (Vlček et al., 2024, modified). **B.** Cross plot diagram of Carbon preference index (CPI) vs. Terrigenous/Aquatic Ratio (TAR) indicating differences in organic matter type between the Kolárovo-4 and Zelený Háj-1 wells. HEBs – hybrid event beds.

As could be seen in Fig. 8A, the samples originating from the Ivanka Fm. in the Kolárovo-4 and consisting of hybrid event beds bear a significantly different signature from the Ivanka Fm. samples of the Zelený Háj-1 well, which show prevalence of short chain n-alkanes. Most of these samples coming from the Zelený Háj-1 do not contain a significant proportion of hybrid event beds. On the other hand, the proportion of n-alkanes is comparable in general to the Vráble Fm. samples from Kolárovo-1 well. A very similar pattern could be observed in Fig. 8B, where the Zelený Háj-1 samples from Ivanka Fm. show significantly lower TAR values and much higher CPI values in comparison to both the Ivanka and Vráble fms. samples taken from Kolárovo-4 well.

## 5. Discussion – deep water mud redeposition affecting authigenic $^{10}Be/^{9}Be$

The synthesis of indices based on facies analysis, biostratigraphy of foraminifers and calcareous nannoplankton, inorganic geochemistry and biomarkers provides a relatively robust basis to explain the anomalously low authigenic $^{10}Be/^{9}Be$ ratios and radiometric ages calculated for the Vráble and Ivanka formations significantly older from independent constraints. All the listed indices reveal that the analyzed succession contains a significant proportion of clastic fine-grained material, redeposited likely from the Middle Miocene formations in deep water environment.

Calcareous nannoplankton fossils point to the source of sediment within the NN6 biostratigraphic zone, which was constrained to 13.5–11.8 Ma (Martini, 1971). The NN6 Zone comprises the Serravallian succession (upper Badenian–Sarmatian) deposited dominantly in marine environment. A common feature of the upper Badenian nannofossils is a higher genus diversity with lower abundances. At the same time, a typical characteristic of calcareous nannofossil assemblage from the Sarmatian age is a less diverse assemblage with higher abundances (Galović, 2017; Galović, 2020; Ćorić, 2021; Hajek-Tadesse et al., 2023). Only blips of endemic taxa occur in the Pannonian stage of the Danube Basin, present even less than during the Sarmatian. Reworked fossils are primarily of the Middle Miocene age, but Lower Miocene, Paleogene, and Cretaceous fossils are present as well.

552 The foraminiferal assemblage obtained from the Ivanka Fm. sediments of the Kolárovo-4 well
553 documents a deep water association resedimented probably from the upper Badenian succession
554 (*Globigerina bulloides*, accompanied with *Cibicidoides* sp., *Bolivina antiqua* in the correlative
555 horizon of Modrany-1 well, Vlček et al. 2020b) except rare occurrences of very shallow water and
556 perhaps Pannonian specimens (*Miliammina* sp.) (Fuchs and Schreiber, 1988; Filipescu et al., 1999;
557 Filipescu and Kaminski, 2008; Hudáčková et al., 2018b). The typical Sarmatian taxa *Elphidium*
558 *hauerinum* and *Porosonion* sp. are poorly preserved in the lower part (cores 8–12 of the Kolárovo-4
559 well). On the other hand, they are more abundant with signs of dissolution or in the form of casts
560 (Fig. 4), which are considered as redeposited. Sediments from the Vráble Fm. in the Kolárovo-4 well
561 provided diversified foraminiferal assemblage of *Elphidium hauerinum* Zone (Harzhauser and Piller,
562 2004; Kováč et al., 2018a), which evidences a lagoonal or marginal marine environment (Fordinál et
563 al., 2006; Kováč et al., 2017) with a possibly decreased salinity.

564 Furthermore, the comparative geochemical analysis of the extensive regional dataset indicates that
565 recycling of material from local sources is a common feature of all Middle Miocene formations up to
566 the lowermost part of the Upper Miocene Ivanka Fm. (geochemical types 2–4). These successions
567 correspond temporally to the four phases of the Danube Basin rifting stage (Šujan et al., 2021b), when
568 formation of half-grabens forced the dominance of local sediment sources. Recycling in the sediment
569 routing pathways persisted until the establishment of the regional depositional system of the paleo-
570 Danube and its Western Carpathian tributaries, which overfilled the Pannonian Basin with turbidite,
571 shelf slope, deltaic, and alluvial sediments, characterized as geochemical type 1. The provenance of
572 the redeposited material was likely in the Middle Miocene successions of the Badenian regional
573 Central Paratethys stage, which accumulated in a considerable thickness in the eastern Danube Basin
574 (Kováč et al., 2018a; Šujan et al., 2021b). Part of the Badenian successions is situated below the
575 Vráble Fm., while other portions must have been exposed already during early Late Miocene. A
576 similar switch in provenance was documented in the Drava, Sava or Makó sub-basins of the

Pannonian Basin System, coinciding with the progradation of the regional drainage system during the postrift geodynamic stage (Szuromi-Korecz et al., 2004; Matošević et al., 2023; 2024).

The hypothesis on how redeposition of older Middle Miocene mud into the younger Sarmatian Vráble and Pannonian Ivanka formations modifies the resulting authigenic $^{10}Be/^{9}Be$ ratios and ages, was tested by a back-calculation of the initial ratio. It is based on the age constraints of 12.6–12.1 Ma for the Vráble Fm. in Kolárovo-4 well. Each natural authigenic $^{10}Be/^{9}Be$ ratio of the eight samples from the cores 9–12 was used for back-calculation of two marginal initial ratio values using 12.6 Ma and 12.1 Ma ages for each sample. The resulting ranges between two marginal values of eight samples from the Vráble Fm. were then used to calculate the weighted mean initial $^{10}Be/^{9}Be$ ratio with the KDX application by Spencer et al. (2017). This value reached $2.64 \pm 0.25 \times 10^{-9}$ and is further referred to as the "Sarmatian" initial ratio, which considers the redeposition of the older mud into the depositional environment according to the assumptions made.

When calculating the ages for the Upper Miocene samples of the Ivanka Fm. using the "Sarmatian" initial ratio (Fig. 2C, Table 1), these samples match in general with the independently constrained age range of ~10.0–9.3 Ma. The ages of samples from the core 8 point to the possibility of somewhat older start of the hybrid event beds deposition. The age generally decreasing upwards follows the trend observed in the below-lying Vráble Fm. The observed pattern is interpreted as a confirmation of the assumption of mud redeposition by HEBs affecting the authigenic $^{10}Be/^{9}Be$ ratios.

Nevertheless, it is worth mentioning that the wide uncertainties of all authigenic $^{10}Be/^{9}Be$ values, reaching high apparent ages at the limits of the method's applicability. This is underscored by the measured sample AMS $^{10}Be/^{9}Be$ ratios, six of them in the range of $10–15 \times 10^{-15}$, which are approaching the level of processing blank AMS $^{10}Be/^{9}Be$ ratios of $7–8 \times 10^{-15}$ (Table 1). This leads to the age overlap of almost all samples when using the "Sarmatian" initial ratio. The laboratory at the Department of Geology and Paleontology of the Comenius University Bratislava employs

nowadays the LGC beryllium ICP-MS standard with $^{10}Be/^{9}Be$ ratios at the levels of $3–4 \times 10^{-15}$ as a carrier during the sample preparation instead of the Scharlau one applied in this study, which will allow to reach better accuracy for the future samples thanks to a roughly two-fold lower $^{10}Be/^{9}Be$ ratio (Merchel et al., 2021).

The back-calculation test indicates that the redeposition process was in general well-balanced for the upper Middle Miocene Vráble Fm., resulting in evenly decreased authigenic $^{10}Be/^{9}Be$ ratios. On the other hand, much higher variability in the Ivanka Fm. implies more dynamic changes in this effect. The sample Kol-4-7b exhibits age within the independent constraints using the lacustrine initial ratio from Šujan et al. (2016), indicating that this sole sample might not be affected by the redeposition in general. Although Kol-4-7b is separated by only a few meters of succession from the sample Kol-4-7a, which was affected by redeposition, the core examples in Fig. 3 demonstrate that depositional processes varied even within a few centimeters of succession, potentially resulting in changes to beryllium isotopic fluxes. However, all remaining samples were affected systematically, which stands out as a proof of pervasive nature of the deep-water redeposition of mud by gravity flows in the whole analyzed succession.

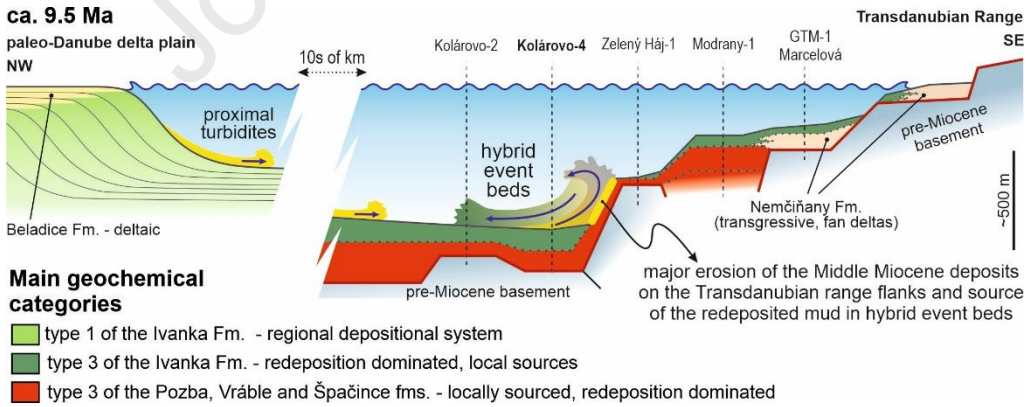


**Fig. 9.** Paleogeographic scenario showing gravity flows sourced from the paleo-Danube depositional system on the northwest, which composition significantly altered by erosion of the Middle Miocene mudstones on the opposite, southeastern side of the basin, resulting in

620 formation of hybrid event beds. Note the high thickness of the type 3 deposits of the Ivanka Fm.
621 below the flanks, and their contrasting low thickness above the flank.

622 The observed basin-fill geometry and sediment distribution in the Ivanka Fm. suggest a
623 paleogeographic scenario depicted in Fig. 9. The formation of hybrid event beds was predisposed by
624 a NE–SW oriented embayment of Lake Pannon, only a few tens of kilometers wide. Turbidity
625 currents, triggered from the prograding shelf slope in the northwest, were confined by the subaquatic
626 foothills of the Transdanubian Range on the basin's southeast flank, leading to erosion and
627 redeposition at the lake bottom. Several million years older formations (possibly the Badenian Pozba
628 and Špačince formations) were exposed due to the earlier Late Miocene rifting, which caused
629 morphological differentiation of the lake floor. This confinement, along with erosion and redeposition
630 by deep-water gravity currents, led to the anomalously thick basin floor deposits in the Kolárovo-4
631 well area (Fig. 9). In contrast, the thin Middle Miocene deposits and hybrid event beds in the basin
632 floor interval of the Zelený Háj-1 well area likely resulted from its position atop a morphological
633 constraint (Fig. 9), which faced significant erosion and a condensed sediment supply from gravity
634 currents.

635 The observed process of deep-water mud redeposition occurred when the normal regressive clastic
636 wedge of the paleo-Danube began prograding across the basin system. Importantly, it demonstrates
637 that normal regressive deep-water deposits could be problematic for authigenic $^{10}Be/^{9}Be$ dating,
638 despite the deltaic part of the normal regressive system being considered suitable for the method
639 (Aherwar et al., 2024). Therefore, basin paleogeography should be carefully considered when
640 developing sampling strategies for authigenic $^{10}Be/^{9}Be$ dating. Narrow confinement caused for
641 example by basin rifting predisposes deep-water redeposition of older mud as extraclasts, while
642 hybrid event beds on an unconfined basin floor are more likely to entrain coeval mud (intraclasts),
643 avoiding significant authigenic $^{10}Be/^{9}Be$ age offsets.

644 The study emphasizes the importance of detailed stratigraphic analysis in a succession to achieve
645 accurate authigenic $^{10}Be/^{9}Be$ dating. Current understanding of the factors influencing this method
646 suggests that integrated multiproxy evidence, such as that presented in this study, can support the
647 conceptual interpretation of paleo-isotopic beryllium fluxes. Nevertheless, facies analysis and
648 sequence stratigraphy remain the most reliable tools for avoiding misleading $^{10}Be/^{9}Be$ dating results,
649 and they cannot be replaced by any other analytical method.

650 ## 6. Conclusion

651 This study provides the first direct evidence of redeposition in a deep-water environment as the cause
652 of significantly older authigenic $^{10}Be/^{9}Be$ radiometric dating results. The proposed hypothesis is
653 process-based, attributing the redeposition of significantly older mud into younger deep-water strata
654 to the hybrid event mechanism. This is supported by multiproxy evidence, including sedimentology,
655 biostratigraphy of reworked nannoplankton and foraminiferal fossil assemblages, inorganic
656 geochemistry from an extensive regional dataset, and organic geochemical indices. This study adds a
657 critical piece to the complex puzzle of understanding the authigenic $^{10}Be/^{9}Be$ isotopic systematics in
658 clastic sediments, which is essential for its effective application in geochronology.

659 Notably, the study reveals an important geochemical signature of the basin fill, which indicates the
660 dominance of sediment redeposition from local sources during and shortly after the Pannonian Basin
661 rifting, while regional sediment routing systems formed later during the overfilling of the basin by
662 sediment supply. The dominance of the recycling of older successions during the rifting stage is a
663 major issue that impedes the use of standard biostratigraphy and could be investigated more precisely,
664 for example, through the analysis of detrital zircons, thanks to the simultaneous volcanic activity.

Journal Pre-proof

## Acknowledgement

The study was supported by the Slovak Research and Development Agency (APVV) under the contracts Nos. APVV-20-0120 and APVV-23-0227. Funded by the EU NextGenerationEU through the Recovery and Resilience Plan for Slovakia under the project No. 09I03-03-V04-0023. ASTER AMS, national facility (CEREGE, Aix-en-Provence), is supported by the INSU/CNRS and IRD and member of AIX MARSEILLE PLATFORMS and REGEF networks. Sofia and Sally Tambarann are thanked for their patience during the artwork preparation.

## References

Aherwar, K., Šujan, M., Amorosi, A., Campo, B., Chyba, A., Tomašových, A., Rózsová, B., Team, A. and Braucher, R., 2024. Low variability of authigenic $^{10}Be/^{9}Be$ across the Holocene Po plain parasequences reveals suitability of dating method for highstand deltaic deposits. Quaternary Science Advances, 15, 100201.

Aherwar, K., Šujan, M., Šarinová, K., Braucher, R., de Leeuw, A., Chyba, A. and AsterTeam, 2021. Applicability of the authigenic $^{10}Be/^{9}Be$ dating to deltaic deposits: Preliminary results from the Slanicul de Buzau section, Pliocene, Romania. EGU General Assembly 2021, online, 19–30 Apr 2021, EGU21-13808, https://doi.org/10.5194/egusphere-egu21-13808.

Aldahan, A.A., Ning, S., Possnert, G., Backman, J. and Boström, K., 1997. $^{10}Be$ records from sediments of the Arctic Ocean covering the past 350 ka. Marine Geology, 144(1–3), 147-162.

Amorosi, A., Bruno, L., Campo, B., Costagli, B., Dinelli, E., Hong, W., Sammartino, I. and Vaiani, S.C., 2020. Tracing clinothem geometry and sediment pathways in the prograding Holocene Po Delta system through integrated core stratigraphy. Basin Research, 32(2), 206-215.

Baas, J.H., Baker, M.L., Malarkey, J., Bass, S.J., Manning, A.J., Hope, J.A., Peakall, J., Lichtman, I.D., Ye, L., Davies, A.G., Parsons, D.R., Paterson, D.M. and Thorne, P.D., 2019. Integrating

field and laboratory approaches for ripple development in mixed sand–clay–EPS. Sedimentology, 66(7), 2749-2768.

Baas, J.H., Best, J.L., Peakall, J. and Wang, M., 2009. A phase diagram for turbulent, transitional, and laminar clay suspension flows. Journal of Sedimentary Research, 79(4), 162-183.

Balázs, A., Magyar, I., Matenco, L., Sztanó, O., Tőkés, L. and Horváth, F., 2018. Morphology of a large paleo-lake: Analysis of compaction in the Miocene-Quaternary Pannonian Basin. Global and Planetary Change, 171, 134-147.

Balco, G., DeJong, B.D., Ridge, J.C., Bierman, P.R. and Rood, D.H., 2021. Atmospherically produced beryllium-10 in annually laminated late-glacial sediments of the North American Varve Chronology. Geochronology, 3(1), 1-33.

Barg, E., Lal, D., Pavich, M.J., Caffee, M.W. and Southon, J.R., 1997. Beryllium geochemistry in soils: evaluation of $^{10}Be/^{9}Be$ ratios in authigenic minerals as a basis for age models. Chemical Geology, 140(3–4), 237-258.

Bourlès, D., Raisbeck, G.M. and Yiou, F., 1989. $^{10}Be$ and $^{9}Be$ in marine sediments and their potential for dating. Geochimica et Cosmochimica Acta, 53(2), 443-452.

Bown, P.R. and Young, J.R., 1998. Techniques. In: P.R. Bown (Ed.), Calcareous nannofossil biostratigraphy. British Micropalaeontological Society, Publications Series. Chapman and Hall, London, pp. 16-28.

Braucher, R., Guillou, V., Bourlès, D.L., Arnold, M., Aumaître, G., Keddadouche, K. and Nottoli, E., 2015. Preparation of ASTER in-house $^{10}Be/^{9}Be$ standard solutions. Nuclear Instruments and Methods in Physics Research Section B: Beam Interactions with Materials and Atoms, 361, 335-340.

Bray, E.E. and Evans, E.D., 1961. Distribution of n-paraffins as a clue to recognition of source beds. Geochimica et Cosmochimica Acta, 22(1), 2-15.

712 Brown, E.T., Edmond, J.M., Raisbeck, G.M., Bourlès, D.L., Yiou, F. and Measures, C.I., 1992a.
713 Beryllium isotope geochemistry in tropical river basins. Geochimica et Cosmochimica Acta,
714 56(4), 1607-1624.
715 Brown, E.T., Measures, C.I., Edmond, J.M., Bourlès, D.L., Raisbeck, G.M. and Yiou, F., 1992b.
716 Continental inputs of beryllium to the oceans. Earth and Planetary Science Letters, 114(1),
717 101-111.
718 Budai, T., Csillag, G., Kercsmár, Z., Selmeczi, I. and Sztanó, O., 2015. Surface geology of Hungary.
719 Explanatory notes to the Geological map of Hungary (1:500 000). Geological and
720 Geophysical Institute of Hungary, Budapest, 66 pp.
721 Cao, Z.-P., Yang, Y., Xu, S., Xu, H., Gu, Z. and Chu, G., 2023. Authigenic beryllium isotopes reveal
722 fluctuations in the East Asian monsoon over the past two millennia. Quaternary Science
723 Reviews, 306, 108043.
724 Carcaillet, J., Bourlès, D.L., Thouveny, N. and Arnold, M., 2004. A high resolution authigenic
725 $^{10}Be/^{9}Be$ record of geomagnetic moment variations over the last 300 ka from sedimentary
726 cores of the Portuguese margin. Earth and Planetary Science Letters, 219(3–4), 397-412.
727 Cicha, I., Rögl, F., Rupp, C. and Čtyroká, J., 1998. Oligocene-Miocene foraminifera of the central
728 Paratethys. Abhandlungen der Senckenbergischen Naturforschenden Gesellschaft, 549, 1-
729 325.
730 Ćorić, S., 2021. Calcareous nannofossils from the middle/upper Miocene succession of Pécs-
731 Danitzpuszta, southern Hungary: cosmopolitan Paratethys and endemic Lake Pannon
732 assemblages. Foldtani Kozlony, 151(3), 253-266.
733 Ćorić, S., Galović, I. and Matošević, M., 2023. New calcareous nannofossils from the Middle to Late
734 Miocene of the North Croatian Basin, Central Paratethys. Journal of Nannoplankton Research,
735 41(1), 1-12.

736 Cranwell, P.A., 1973. Chain-length distribution of n-alkanes from lake sediments in relation to post-
737 glacial environmental change. Freshwater Biology, 3(3), 259-265.
738 Cranwell, P.A., Eglinton, G. and Robinson, N., 1987. Lipids of aquatic organisms as potential
739 contributors to lacustrine sediments—II. Organic Geochemistry, 11(6), 513-527.
740 Deng, K., Rickli, J., Suhrhoff, T.J., Du, J., Scholz, F., Severmann, S., Yang, S., McManus, J. and
741 Vance, D., 2023. Dominance of benthic fluxes in the oceanic beryllium budget and
742 implications for paleo-denudation records. Science Advances, 9(23), eadg3702.
743 Dixon, J.L., Chadwick, O.A. and Pavich, M.J., 2018. Climatically controlled delivery and retention
744 of meteoric $^{10}$Be in soils. Geology, 46(10), 899-902.
745 Ficken, K.J., Li, B., Swain, D.L. and Eglinton, G., 2000. An n-alkane proxy for the sedimentary input
746 of submerged/floating freshwater aquatic macrophytes. Organic Geochemistry, 31(7), 745-
747 749.
748 Filipescu, S. and Kaminski, M.A., 2008. Re-discovering Entzia, an agglutinated foraminifer from the
749 Transylvanian salt marshes. In: M.A. Kaminski and S. Filipescu (Eds.), Proceedings of the
750 Eighth International Workshop on Agglutinated Foraminifera, Grzybowski Foundation
751 Special Publication, pp. 29-35.
752 Filipescu, S., Popa, M. and Wanek, F., 1999. The significance of some Sarmatian faunas from the
753 southwestern part of the Padurea Craiului Mountains (Romania). Acta Palaeontologica
754 Romaniae, 2, 163-169.
755 Fonnesu, M., Felletti, F., Haughton, P.D.W., Patacci, M. and McCaffrey, W.D., 2018. Hybrid event
756 bed character and distribution linked to turbidite system sub-environments: The North
757 Apennine Gottero Sandstone (north-west Italy). Sedimentology, 65(1), 151-190.
758 Fordinál, K., Zágoršek, K. and Zlinská, A., 2006. Early Sarmatian biota in the northern part of the
759 Danube Basin (Slovakia). Geologica Carpathica, 57(2), 123-130.

760 Fuchs, T. and Schreiber, O.S., 1988. Agglutinated foraminiferal assemblages as indicators of
761 environmental changes in the early Pannonian (Late Miocene) of the Vienna Basin. In: F.
762 Rögl and F.M. Gradstein (Eds.), Second Workshop on Agglutinated Foraminifera.
763 Abhandlungen des Geoligischen Bundesanstalt, Wien, 41, pp. 61-71.
764 Galović, I., 2017. Sarmatian calcareous nannofossil assemblages in the SW Paratethyan marginal
765 marine environments: Implications for palaeoceanography and the palaeoclimate. Progress in
766 Oceanography, 156, 209-220.
767 Galović, I., 2020. Sarmatian biostratigraphy of a marginal sea in northern Croatia based on calcareous
768 nannofossils. Marine Micropaleontology, 161, 101928.
769 Gocke, M., Kuzyakov, Y. and Wiesenberg, G.L.B., 2013. Differentiation of plant derived organic
770 matter in soil, loess and rhizoliths based on n-alkane molecular proxies. Biogeochemistry,
771 112(1), 23-40.
772 Graham, I.J., Ditchburn, R.G. and Whitehead, N.E., 1998. $^{10}$Be spikes in Plio–Pleistocene
773 cyclothems, Wanganui Basin, New Zealand: identification of the local flooding surface (LFS).
774 Sedimentary Geology, 122(1), 193-215.
775 Graham, I.J., Ditchburn, R.G. and Whitehead, N.E., 2001. Be isotope analysis of a 0–500 ka loess–
776 paleosol sequence from Rangitatau East, New Zealand. Quaternary International, 76–77, 29-
777 42.
778 Grill, R., 1941. Stratigraphische Untersuchungen mit Hilfe von Mikrofaunen im Wiener Becken und
779 den benachbarten Molasse-Anteilen. Oel und Kohle, 37, 595-602.
780 Hajek-Tadesse, V., Wacha, L., Horvat, M., Galović, I., Bakrač, K., Grizelj, A., Mandic, O. and
781 Reichenbacher, B., 2023. New evidence for Early Miocene palaeoenvironmental changes in
782 the North Croatian Basin: Insights implicated by microfossil assemblages. Geobios, 77, 1-25.

Journal Pre-proof

783 Harzhauser, M. and Mandic, O., 2008. Neogene lake systems of Central and South-Eastern Europe:
784 Faunal diversity, gradients and interrelations. Palaeogeography Palaeoclimatology
785 Palaeoecology, 260(3-4), 417-434.
786 Harzhauser, M., Mandic, O., Kranner, M., Lukeneder, P., Kern, A.K., Gross, M., Carnevale, G. and
787 Jawecki, C., 2018. The Sarmatian/Pannonian boundary at the western margin of the Vienna
788 Basin (City of Vienna, Austria). Austrian Journal of Earth Sciences, 111(1), 26-"47, A1-A4".
789 Harzhauser, M. and Piller, W., 2004. Integrated stratigraphy of the Sarmatian (Upper Middle
790 Miocene) in the western Central Paratethys. Stratigraphy, 1(1), 65-86.
791 Haughton, P., Davis, C., McCaffrey, W. and Barker, S., 2009. Hybrid sediment gravity flow deposits
792 - Classification, origin and significance. Marine and Petroleum Geology, 26(10), 1900-1918.
793 Hayward, B.W., Le Coze, F., Vachard, D. and Gross, O., 2023. World Foraminifera Database.
794 Accessed at https://www.marinespecies.org/foraminifera on 2023–04–27 and 2024–07–27.
795 Herron, M.M., 1988. Geochemical classification of terrigenous sands and shales from core or log
796 data. Journal of Sedimentary Petrology, 58, 820-829.
797 Holcová, K.n., 1999. Postmortem transport and resedimentation of foraminiferal tests: relations to
798 cyclical changes of foraminiferal assemblages. Palaeogeography, Palaeoclimatology,
799 Palaeoecology, 145(1–3), 157-182.
800 Horváth, F., Bada, G., Szafián, P., Tari, G., Ádám, A. and Cloetingh, S., 2006. Formation and
801 deformation of the Pannonian Basin: Constraints from observational data. In: D.G. Gee and
802 R.A. Stephenson (Eds.), European Lithosphere Dynamics, Geological Society of London
803 Memoir, pp. 191-206.
804 Hudáčková, N., Holcová, K., Halásová, E., Kováčová, M., Doláková, N., Trubač, J., Rybár, S.,
805 Ruman, A., Stárek, D., Šujan, M., Jamrich, M. and Kováč, M., 2020. The Pannonian Basin
806 System northern margin paleogeography, climate, and depositional environments in the time

range during MMCT (Central Paratethys, Novohrad-Nógrád Basin, Slovakia). Palaeontologia Electronica, 23(3), 1-35.

Hudáčková, N., Kováč, M., Ruman, A., Halasová, E., Jamrich, M., Kováčová, M., Rybár, S., Šujan, M. and Šarinová, K., 2018a. Biostratigraphic study: Špačince-4 and Dubove-2 wells. Manuscript, archive of the Nafta company. Department of Geology and Paleontology, Faculty of Natural Sciences, Comenius University Bratislava.

Hudáčková, N., Soták, J., Ruman, A., Rybár, S. and Milovský, R., 2018b. Marsh-type agglutinated foraminifera from UpperMiocene sediments of the Danube Basin. Micropaleontology, 64(5-6), 481-492.

Chmeleff, J., von Blanckenburg, F., Kossert, K. and Jakob, D., 2010. Determination of the $^{10}$Be half-life by multicollector ICP-MS and liquid scintillation counting. Nuclear Instruments and Methods in Physics Research, Section B: Beam Interactions with Materials and Atoms, 268(2), 192-199.

Jena, P.S., Bhushan, R., Ajay, S., Bharti, N. and Sudheer, A.K., 2022. $^{10}$Be depositional flux variation in the central Indian Ocean during the last 43 ka. Science of The Total Environment, 802, 149808.

Jena, P.S., Bhushan, R., Ajay, S., Dabhi, A.J., Gaddam, M. and Sudheer, A.K., 2023a. Applicability of meteoric $^{10}$Be in dating marine sediment cores. Marine Chemistry, 254, 104275.

Jena, P.S., Bhushan, R., Ajay, S. and Sudheer, A.K., 2023b. Spatial heterogeneity in beryllium isotopic distribution in the Indian Ocean. Geochimica et Cosmochimica Acta, 342, 128-136.

Jeong, A., Seong, Y.B., Gootee, B.F., Yu, B.Y. and Cheung, S.Y., 2023. Application and limitations of the authigenic $^{10}$Be/$^{9}$Be and meteoric $^{10}$Be inventory in Bouse Formation along the lower Colorado River corridor, southwestern USA. Episodes, 46(1), 85-97.

Johannessen, E.P. and Steel, R.J., 2005. Shelf-margin clinoforms and prediction of deepwater sands. Basin Research, 17(4), 521-550.

832 Kane, I.A. and Ponten, A.S.M., 2012. Submarine transitional flow deposits in the Paleogene Gulf of
833 Mexico. Geology, 40(12), 1119-1122.
834 Kázmér, M., 1990. Birth, life and death of the Pannonian Lake. Palaeogeography, Palaeoclimatology,
835 Palaeoecology, 79(1–2), 171-188.
836 Keith, J.F., Vass, D., Kanes, W.H., Pereszlényi, M., Kováč, M. and Kral', J., 1989. Sedimentary basins
837 of Slovakia, Part II. Final report on the Hydrocarbon pontenial of Danube Lowland Basin, 1.
838 Manuscript Univ. South Carolina, ESRI, Technical Report 89-0019.
839 Kong, W.Y., Zhou, L.P. and AsterTeam, 2021. Tracing Water Masses and Assessing Boundary
840 Scavenging Intensity With Beryllium Isotopes in the Northern South China Sea. Journal of
841 Geophysical Research: Oceans, 126(7), e2021JC017236.
842 Korschinek, G., Bergmaier, A., Faestermann, T., Gerstmann, U.C., Knie, K., Rugel, G., Wallner, A.,
843 Dillmann, I., Dollinger, G., Lierse von Gosstomski, C., Kossert, K., Maiti, M., Poutivtsev, M.
844 and Remmert, A., 2010. A new value for the $^{10}$Be half-life by heavyion elastic recoil detection
845 and liquid scintillation counting. . Nuclear Instruments and Methods in Physics Research
846 Section B: Beam Interactions with Materials and Atoms, 268(2), 187-191.
847 Kováč, M., Halásová, E., Hudáčková, N., Holcová, K., Hyžný, M., Jamrich, M. and Ruman, A.,
848 2018a. Towards better correlation of the Central Paratethys regional time scale with the
849 standard geological time scale of the Miocene Epoch. Geologica Carpathica, 69(3), 283-300.
850 Kováč, M., Hudáčková, N., Halásová, E., Kováčová, M., Holcová, K., Oszczypko-Clowes, M., Báldi,
851 K., Less, G., Nagymarosy, A., Ruman, A., Klučiar, T. and Jamrich, M., 2017. The Central
852 Paratethys palaeoceanography: A water circulation model based on microfossil proxies,
853 climate, and changes of depositional environment. Acta Geologica Slovaca, 9(2), 75-114.
854 Kováč, M., Rybár, S., Halásová, E., Hudáčková, N., Šarinová, K., Šujan, M., Baranyi, V., Kováčová,
855 M., Ruman, A., Klučiar, T. and Zlinská, A., 2018b. Changes in Cenozoic depositional
856 environment and sediment provenance in the Danube Basin. Basin Research, 30(1), 97-131.

857 Krishnaswami, S., Mangini, A., Thomas, J.H., Sharma, P., Cochran, J.K., Turekian, K.K. and Parker,
858 P.D., 1982. $^{10}$Be and Th isotopes in manganese nodules and adjacent sediments: Nodule
859 growth histories and nuclide behavior. Earth and Planetary Science Letters, 59(2), 217-234.
860 Kusakabe, M. and Ku, T.-L., 1984. Incorporation of Be isotopes and other trace metals into marine
861 ferromanganese deposits. Geochimica et Cosmochimica Acta, 48(11), 2187-2193.
862 Kusakabe, M., Ku, T.L., Southon, J.R., Vogel, J.S., Nelson, D.E., Measures, C.I. and Nozaki, Y.,
863 1987. Distribution of $^{10}$Be and $^{9}$Be in the Pacific Ocean. Earth and Planetary Science Letters,
864 82(3), 231-240.
865 Lebatard, A.E., Bourlès, D.L., Duringer, P., Jolivet, M., Braucher, R., Carcaillet, J., Schuster, M.,
866 Arnaud, N., Monié, P., Lihoreau, F., Likius, A., Mackaye, H.T., Vignaud, P. and Brunet, M.,
867 2008. Cosmogenic nuclide dating of Sahelanthropus tchadensis and Australopithecus
868 bahrelghazali: Mio-Pliocene hominids from Chad. Proceedings of the National Academy of
869 Sciences of the United States of America, 105(9), 3226-3231.
870 Lin, Z., Strauss, H., Peckmann, J., Roberts, A.P., Lu, Y., Sun, X., Chen, T. and Harzhauser, M., 2023.
871 Seawater sulphate heritage governed early Late Miocene methane consumption in the long-
872 lived Lake Pannon. Communications Earth & Environment, 4(1), 207.
873 Lisé-Pronovost, A., Fletcher, M.-S., Simon, Q., Jacobs, Z., Gadd, P.S., Heslop, D., Herries, A.I.R.,
874 Yokoyama, Y. and team, A., 2021. Chronostratigraphy of a 270-ka sediment record from Lake
875 Selina, Tasmania: Combining radiometric, geomagnetic and climatic dating. Quaternary
876 Geochronology, 62, 101152.
877 Magyar, I., Geary, D.H. and Müller, P., 1999. Paleogeographic evolution of the Late Miocene Lake
878 Pannon in Central Europe. Palaeogeography, Palaeoclimatology, Palaeoecology, 147(3–4),
879 151-167.

Journal Pre-proof

880 Magyar, I., Lantos, M., Ujszaszi, K. and Kordos, L., 2007. Magnetostratigraphic, seismic and
881 biostratigraphic correlations of the Upper Miocene sediments in the northwestern Pannonian
882 Basin System. Geologica Carpathica, 58(3), 277-290.
883 Magyar, I., Radivojevic, D., Sztano, O., Synak, R., Ujszaszi, K. and Pocsik, M., 2013. Progradation
884 of the paleo-Danube shelf margin across the Pannonian Basin during the Late Miocene and
885 Early Pliocene. Global and Planetary Change, 103, 168-173.
886 Martini, E., 1971. Standard Tertiary and Quaternary calcareous nannoplankton zonation. In: A.
887 Farinacci (Ed.), Proceedings of the Second Planktonic Conference Roma 1970, Edizioni
888 Tecnoscienza, Rome, pp. 739-785.
889 Matošević, M., Garzanti, E., Šuica, S., Bersani, D., Marković, F., Razum, I., Grizelj, A., Petrinjak,
890 K., Kovačić, M. and Pavelić, D., 2024. The Alps as the main source of sand for the Late
891 Miocene Lake Pannon (Pannonian Basin, Croatia). Geologia Croatica, 77(2), 69-83.
892 Matošević, M., Marković, F., Bigunac, D., Šuica, S., Krizmanić, K., Perković, A., Kovačić, M. and
893 Pavelić, D., 2023. Petrography of the Upper Miocene sandstones from the North Croatian
894 Basin: Understanding the genesis of the largest reservoirs in the southwestern part of the
895 Pannonian Basin System. Geologica Carpathica, 74(2), 155-179.
896 McLennan, S.M., 2001. Relationships between the trace element composition of sedimentary rocks
897 and upper continental crust. Geochemistry, Geophysics, Geosystems, 2(4).
898 McLennan, S.M., Hemming, S., McDaniel, D.K. and Hanson, G.N., 1993. Geochemical approaches
899 to sedimentation, provenance, and tectonics. In: M.J. Johnsson and A. Basu (Eds.), Processes
900 Controlling the Composition of Clastic Sediments. Geological Society of America, pp. 0.
901 Measures, C.I. and Edmond, J.M., 1982. Beryllium in the water column of the central North Pacific.
902 Nature, 297(5861), 51-53.

Journal Pre-proof

903 Measures, C.I., Ku, T.L., Luo, S., Southon, J.R., Xu, X. and Kusakabe, M., 1996. The distribution of
904 $^{10}$Be and $^{9}$Be in the South Atlantic. Deep Sea Research Part I: Oceanographic Research
905 Papers, 43(7), 987-1009.
906 Merchel, S., Beutner, S., Opel, T., Rugel, G., Scharf, A., Tiessen, C., Weiß, S. and Wetterich, S.,
907 2019. Attempts to understand potential deficiencies in chemical procedures for AMS. Nuclear
908 Instruments and Methods in Physics Research Section B: Beam Interactions with Materials
909 and Atoms, 456, 186-192.
910 Merchel, S., Braucher, R., Lachner, J. and Rugel, G., 2021. Which is the best 9Be carrier for $^{10}$Be/$^{9}$Be
911 accelerator mass spectrometry? MethodsX, 8, 101486.
912 Meyers, P.A. and Ishiwatari, R., 1993. Lacustrine organic geochemistry-an overview of indicators of
913 organic matter sources and diagenesis in lake sediments. Organic Geochemistry, 20(7), 867-
914 900.
915 McHargue, L.R., Jull, A.J.T. and Cohen, A., 2011. Measurement of $^{10}$Be from Lake Malawi (Africa)
916 drill core sediments and implications for geochronology. Palaeogeography,
917 Palaeoclimatology, Palaeoecology, 303(1–4), 110-119.
918 Nagender Nath, B., Aldahan, A., Possnert, G., Selvaraj, K., Mascarenhas-Pereira, M.B.L. and Chen,
919 C.T.A., 2007. $^{10}$Be variation in surficial sediments of the Central Indian Basin. Nuclear
920 Instruments and Methods in Physics Research Section B: Beam Interactions with Materials
921 and Atoms, 259(1), 610-615.
922 Patruno, S. and Helland-Hansen, W., 2018. Clinoforms and clinoform systems: Review and dynamic
923 classification scheme for shorelines, subaqueous deltas, shelf edges and continental margins.
924 Earth-Science Reviews, 185, 202-233.
925 Portenga, E.W., Bierman, P.R., Trodick, C.D., Jr., Greene, S.E., DeJong, B.D., Rood, D.H. and
926 Pavich, M.J., 2019. Erosion rates and sediment flux within the Potomac River basin quantified
927 over millennial timescales using beryllium isotopes. GSA Bulletin, 131(7-8), 1295-1311.

928 Rahaman, W., Wittmann, H. and von Blanckenburg, F., 2017. Denudation rates and the degree of
929 chemical weathering in the Ganga River basin from ratios of meteoric cosmogenic $^{10}$Be to
930 stable 9Be. Earth and Planetary Science Letters, 469, 156-169.
931 Riboulleau, A., Bout-Roumazeilles, V., Tribovillard, N., Guillot, F. and Recourt, P., 2014. Testing
932 provenance diagrams: Lessons from the well-constrained Cariaco Basin. Chemical Geology,
933 389, 91-103.
934 Ruman, A., Ćorić, S., Halásová, E., Harzhauser, M., Hudáčková, N., Jamrich, M., Palzer-Khomenko,
935 M., Kranner, M., Mandic, O., Rybár, S., Šimo, V., Šujan, M. and Kováč, M., 2021. The
936 "Rzehakia beds" on the northern shelf of the Pannonian Basin: biostratigraphic and
937 palaeoenvironmental implications. Facies, 67(1).
938 Rybár, S., Halásová, E., Hudáčková, N., Kováč, M., Kováčová, M., Šarinová, K. and Šujan, M., 2015.
939 Biostratigraphy, sedimentology and paleoenvironments of the northern Danube Basin:
940 Ratkovce 1 well case study. Geologica Carpathica, 66(1), 51-67.
941 Rybár, S. and Kotulová, J., 2023. Petroleum play types and source rocks in the Pannonian basin,
942 insight from the Slovak part of the Danube Basin. Marine and Petroleum Geology, 149,
943 106092.
944 Rybár, S., Kováč, M., Šarinová, K., Halásová, E., Hudáčková, N., Šujan, M., Kováčová, M., Ruman,
945 A. and Klučiar, T., 2016. Neogene changes in Paleogeography, Paleoenvironment and the
946 Provenance of sediment in the Northern Danube Basin. Bulletin of Geosciences, 91(2), 367-
947 398.
948 Rybár, S., Šarinová, K., Jourdan, F., Mayers, C. and Sliva, Ľ., 2024. Middle Miocene volcanic flare
949 up preceding and synchronous with the Langhian/Serravallian sea-level decline in the North
950 Pannonian Basin: Insights from 40Ar/39Ar dating, geo-seismic analysis and 3D visualization
951 of the subterranean Kráľová stratovolcano. Basin Research, 36(1), e12844.

952 Rybár, S., Šarinová, K., Sant, K., Kuiper, K.F., Kováčová, M., Vojtko, R., Reiser, M.K., Fordinál,
953 K., Teodoridis, V., Nováková, P. and Vlček, T., 2019. New 40Ar/39Ar, fission track and
954 sedimentological data on a middle Miocene tuff occurring in the Vienna Basin: implications
955 for the North-Western Central Paratethys region. Geologica Carpathica, 70(5), 386-404.
956 Salocchi, A.C., Krawielicki, J., Eglinton, T.I., Fioroni, C., Fontana, D., Conti, S. and Picotti, V., 2021.
957 Biomarker constraints on Mediterranean climate and ecosystem transitions during the Early-
958 Middle Miocene. Palaeogeography, Palaeoclimatology, Palaeoecology, 562, 110092.
959 Sharma, P., Mahannah, R., Moore, W.S., Ku, T.L. and Southon, J.R., 1987. Transport of $^{10}$Be and
960 $^{9}$Be in the ocean. Earth and Planetary Science Letters, 86(1), 69-76.
961 Sharma, P. and Somayajulu, B.L.K., 1982. $^{10}$Be dating of large manganese nodules from world
962 oceans. Earth and Planetary Science Letters, 59(2), 235-244.
963 Schieber, J., 1998. Shales and Mudstones. In: J. Schieber, W. Zimmerle and P.S. Sethi (Eds.), I. Basin
964 Studies, Sedimentology and Paleontology. Schweizerbart, Stuttgart, pp. 131-146.
965 Simon, Q., Suganuma, Y., Okada, M. and Haneda, Y., 2019. High-resolution $^{10}$Be and paleomagnetic
966 recording of the last polarity reversal in the Chiba composite section: Age and dynamics of
967 the Matuyama–Brunhes transition. Earth and Planetary Science Letters, 519, 92-100.
968 Singleton, A.A., Schmidt, A.H., Bierman, P.R., Rood, D.H., Neilson, T.B., Greene, E.S., Bower, J.A.
969 and Perdrial, N., 2017. Effects of grain size, mineralogy, and acid-extractable grain coatings
970 on the distribution of the fallout radionuclides $^{7}$Be, $^{10}$Be, $^{137}$Cs, and $^{210}$Pb in river sediment.
971 Geochimica et Cosmochimica Acta, 197, 71-86.
972 Spencer, C.J., Yakymchuk, C. and Ghaznavi, M., 2017. Visualising data distributions with kernel
973 density estimation and reduced chi-squared statistic. Geoscience Frontiers, 8(6), 1247-1252.
974 Stow, D.A., 2005. Sedimentary Rocks in the Field. A Colour Guide. Manson Publishing, London,
975 320 pp.

Journal Pre-proof

976 Suhrhoff, T.J., Rickli, J., Christl, M., Vologina, E.G., Pham, V., Belhadj, M., Sklyarov, E.V., Jeandel,
977 C. and Vance, D., 2022. Source to sink analysis of weathering fluxes in Lake Baikal and its
978 watershed based on riverine fluxes, elemental lake budgets, REE patterns, and radiogenic (Nd,
979 Sr) and $^{10}Be/^{9}Be$ isotopes. Geochimica et Cosmochimica Acta, 321, 133-154.
980 Sumner, E.J., Talling, P.J. and Amy, L.A., 2009. Deposits of flows transitional between turbidity
981 current and debris flow. Geology, 37(11), 991-994.
982 Sztanó, O., Kováč, M., Magyar, I., Šujan, M., Fodor, L., Uhrin, A., Rybár, S., Csillag, G. and Tokés,
983 L., 2016a. Late Miocene sedimentary record of the Danube/Kisalföld Basin: Interregional
984 correlation of depositional systems, stratigraphy and structural evolution. Geologica
985 Carpathica, 67(6), 525-542.
986 Sztanó, O., Szafian, P., Magyar, I., Horanyi, A., Bada, G., Hughes, D.W., Hoyer, D.L. and Wallis,
987 R.J., 2013. Aggradation and progradation controlled clinothems and deep-water sand delivery
988 model in the Neogene Lake Pannon, Mako Trough, Pannonian Basin, SE Hungary. Global
989 and Planetary Change, 103, 149-167.
990 Sztanó, O., Šujan, M. and Tőkés, L., 2016b. What's common in Želiezovce Depression, Slovakia and
991 Makó Trough, Hungary? In: M. Šujan (Ed.), 10th Environmental, Structural and
992 Stratigraphical Evolution of the Western Carpathians, 1st - 2nd December 2016, Bratislava,
993 pp. 109-110.
994 Szuromi-Korecz, A., Süto-Szentai, M. and Magyar, I., 2004. Biostratigraphic revision of the Hód-I
995 well: Hungary's deepest borehole failed to reach the base of the Upper Miocene Pannonian
996 stage. Geologica Carpathica, 55(6), 475-485.
997 Šarinová, K., Hudáčková, N., Rybár, S., Jamrich, M., Jourdan, F., Frew, A., Mayers, C., Ruman, A.,
998 Subová, V. and Sliva, Ľ., 2021a. 40Ar/39Ar dating and palaeoenvironments at the boundary
999 of the early-late Badenian (Langhian-Serravallian) in the northwest margin of the Pannonian
1000 basin system. Facies, 67(4).

1001 Šarinová, K., Rybár, S., Halásová, E., Hudáčková, N., Jamrich, M., Kováčová, M. and Šujan, M.,
1002 2018. Integrated biostratigraphical, sedimentological and provenance analyses with
1003 implications for lithostratigraphic ranking: The Miocene Komjatice depression of the Danube
1004 Basin. Geologica Carpathica, 69(4), 382-409.
1005 Šarinová, K., Rybár, S., Jourdan, F., Frew, A., Mayers, C., Kováčová, M., Lichtman, B., Nováková,
1006 P. and Kováč, M., 2021b. 40Ar/Ar39 geochronology of Burdigalian paleobotanical localities
1007 in the Central Paratethys (south Slovakia). Geologica Acta, 19, 1-19.
1008 Šujan, M., 2024. A list of publications applying authigenic $^{10}Be/^{9}Be$ dating method. Mendeley Data,
1009 V1, 29. August 2024, https://doi.org/10.17632/7994s3f4pb.1.
1010 Šujan, M., Aherwar, K., Chyba, A., Rózsová, B., Braucher, R., Šujan, M., Šipka, F. and AsterTeam,
1011 2024. Sedimentological and geochronological data for the fan deltaic Nemčiňany Formation,
1012 Upper Miocene, Danube Basin (Slovakia). Mendeley Data, V3,
1013 https://doi.org/10.17632/svr45t2xtj.3.
1014 Šujan, M., Aherwar, K., Vojtko, R., Braucher, R., Šarinová, K., Chyba, A., Hók, J., Grizelj, A., Pipík,
1015 R., Lalinská-Voleková, B., Rózsová, B. and Team, A., 2023a. Application of the authigenic
1016 $^{10}Be/^{9}Be$ dating to constrain the age of a long-lived lake and its regression in an isolated
1017 intermontane basin: The case of Late Miocene Lake Turiec, Western Carpathians.
1018 Palaeogeography, Palaeoclimatology, Palaeoecology, 628, 111746.
1019 Šujan, M., Braucher, R., Chyba, A., Vlačiky, M., Aherwar, K., Rózsová, B., Fordinál, K., Maglay, J.,
1020 Nagy, A., Moravcová, M. and AsterTeam, 2023b. Mud redeposition during river incision as
1021 a factor affecting authigenic $^{10}Be/^{9}Be$ dating: Early Pleistocene large mammal fossil-bearing
1022 site Nová Vieska, eastern Danube Basin. Journal of Quaternary Science,
1023 https://doi.org/10.1002/jqs.3482.
1024 Šujan, M., Braucher, R., Kováč, M., Bourlès, D.L., Rybár, S., Guillou, V. and Hudáčková, N., 2016.
1025 Application of the authigenic $^{10}Be/^{9}Be$ dating method to Late Miocene–Pliocene sequences in

the northern Danube Basin (Pannonian Basin System): Confirmation of heterochronous evolution of sedimentary environments. Global and Planetary Change, 137, 35-53.

Šujan, M., Braucher, R., Mandic, O., Fordinál, K., Brixová, B., Pipík, R.K., Šimo, V., Jamrich, M., Rybár, S., Klučiar, T., Team, A., Ruman, A., Zvara, I. and Kováč, M., 2021a. Lake Ppannon transgression on the westernmost tip of the Carpathians constrained by biostratigraphy and authigenic $^{10}Be/^{9}Be$ dating (central Europe). Rivista Italiana di Paleontologia e Stratigrafia, 127(3), 627-653.

Šujan, M., Rybár, S., Kováč, M., Bielik, M., Majcin, D., Minár, J., Plašienka, D., Nováková, P. and Kotulová, J., 2021b. The polyphase rifting and inversion of the Danube Basin revised. Global and Planetary Change, 196, 103375.

Šujan, M., Šarinová, K., Hók, J., Vlček, T., Ruman, A., Jamrich, M., Kováčová, M., Droppa, D.M., Fordinál, K., Nagy, A., Moravcová, M., Sztanó, O. and Kováč, M., 2025. Miocene to Quaternary evolution of the northern Danube Basin: A review of geodynamics, depositional systems and stratigraphy. In: G.C. Tari et al. (Eds.), The Miocene Extensional Pannonian Superbasin, Volume 1: Regional Geology. Geological Society, London, Special Publications, pp. SP554-2024-66.

Talling, P.J., Masson, D.G., Sumner, E.J. and Malgesini, G., 2012. Subaqueous sediment density flows: Depositional processes and deposit types. Sedimentology, 59(7), 1937-2003.

Tan, S.H. and Horlick, G., 1987. Matrix-effect observations in inductively coupled plasma mass spectrometry. Journal of Analytical Atomic Spectrometry, 2(8), 745-763.

Vlček, T., Hudáčková, N., Jamrich, M., Halásová, E., Franců, J., Nováková, P., Kováčová, M. and Kováč, M., 2020a. Hydrocarbon potential of the Oligocene and Miocene sediments from the Modrany-1 and Modrany-2 wells (Danube Basin, Slovakia). Acta Geologica Slovaca, 12(1), 43-55.

Journal Pre-proof

1050 Vlček, T., Kováčová, M., Šarinová, K., Rybár, S., Hudáčková, N., Ruman, A., Jamrich, M. and
1051 Franců, J., 2022. Multiproxy constraints on Central Paratethys Sea and Lake Pannon
1052 paleoclimate and paleoenvironment transitions during the Middle-Late Miocene (Danube
1053 Basin, Slovakia). Palaeogeography, Palaeoclimatology, Palaeoecology, 600, 111058.
1054 Vlček, T., Šarinová, K., Kováčová, M., Sztanó, O. and Šujan, M., 2024. Sources and composition of
1055 organic matter as a tool for understanding the complex variation in paleoenvironments and
1056 the connectivity of an epicontinental basin: The Miocene in the northern Pannonian Basin.
1057 Sedimentary Geology, 470, 106721.
1058 Vlček, T., Šarinová, K., Rybár, S., Hudáčková, N., Jamrich, M., Šujan, M., Franců, J., Nováková, P.,
1059 Sliva, Ľ., Kováč, M. and Kováčová, M., 2020b. Paleoenvironmental evolution of Central
1060 Paratethys Sea and Lake Pannon during the Cenozoic. Palaeogeography, Palaeoclimatology,
1061 Palaeoecology, 559, 109892.
1062 von Blanckenburg, F., Bouchez, J. and Wittmann, H., 2012. Earth surface erosion and weathering
1063 from the $^{10}$Be (meteoric)/$^{9}$Be ratio. Earth and Planetary Science Letters, 351-352, 295-305.
1064 von Blanckenburg, F. and O'Nions, R.K., 1999. Response of beryllium and radiogenic isotope ratios
1065 in Northern Atlantic Deep Water to the onset of northern hemisphere glaciation. Earth and
1066 Planetary Science Letters, 167(3-4), 175-182.
1067 Willenbring, J.K. and Von Blanckenburg, F., 2010a. Long-term stability of global erosion rates and
1068 weathering during late-Cenozoic cooling. Nature, 465(7295), 211-214.
1069 Willenbring, J.K. and von Blanckenburg, F., 2010b. Meteoric cosmogenic Beryllium-10 adsorbed to
1070 river sediment and soil: Applications for Earth-surface dynamics. Earth-Science Reviews,
1071 98(1-2), 105-122.
1072 Wittmann, H., Oelze, M., Roig, H. and von Blanckenburg, F., 2018. Are seasonal variations in river-
1073 floodplain sediment exchange in the lower Amazon River basin resolvable through meteoric
1074 cosmogenic $^{10}$Be to stable $^{9}$Be ratios? Geomorphology, 322, 148-158.

1075 Wittmann, H., von Blanckenburg, F., Bouchez, J., Dannhaus, N., Naumann, R., Christl, M. and
1076 Gaillardet, J., 2012. The dependence of meteoric $^{10}Be$ concentrations on particle size in
1077 Amazon River bed sediment and the extraction of reactive $^{10}Be/^{9}Be$ ratios. Chemical Geology,
1078 318–319, 126-138.
1079 Wittmann, H., von Blanckenburg, F., Mohtadi, M., Christl, M. and Bernhardt, A., 2017. The
1080 competition between coastal trace metal fluxes and oceanic mixing from the $^{10}Be/^{9}Be$ ratio:
1081 Implications for sedimentary records. Geophysical Research Letters, 44(16), 8443-8452.
1082 Zima, D., Horányi, A., Molnár, G. and Sztanó, O., 2019. Hybrid event beds in lacustrine confined
1083 turbidite systems, Pannonian Basin, 34$^{th}$ International Meeting of Sedimentology, Rome,
1084 Abstract Book, ISBN 978-88-944576-2-9. Session 4.B - 1844.

Journal Pre-proof

# Supplementary material

**Supplementary Table S1.** A list of stratigraphic important calcareous nannofossils determined in the studied samples. Not mentioned samples were barren.

| **Core** | **D** | **Zone/ Subzone** | **Event** |
|---|---|---|---|
| Kol-4-6a | N | NN6 | *Reticulofenestra pseudoumbilicus*, *R. producta*, *Orthorhabdus rugosus*, reworking |
| Kol-4-7a | N | ?Pannonian/NN6 | ?*Isolithus semenenkoii*, *Orthorhabdus serratus*, *Umbilicosphaera jafari*, *Helicosphaera carteri*, reworking |
| Kol-4-8c | N | ?Pannonian/NN6 | *?I. semenenkoii*, *?Noelaerhabdus bozinovicae*, *Sphenolithus abies*, *Calcidiscus tropicus*, *Coccolithus miopelagicus*, *R. pseudoumbilicus*, reworking |
| Kol-4-9b | N | ?Pannonian/NN6 | *?N. bozinovicae*, *Helicosphaera walbersdorfensis*, *S. abies*, *C. tropicus*, *C. miopelagicus*, *R. pseudoumbilicus*, *Syracosphaera pulchra*, *U. jafari*, *Sphenolithus heteromorphus*, reworking |
| Kol-4-10b | N | NN6 | *R. producta*, *R. pseudoumbilicus*, *Calcidiscus macintyrei*, *C. tropicus*, *C. miopelagicus*, *S. heteromorphus*, reworking |
| Kol-4-11b | N | NN6 | *O. rugosus*, *S. abies*, *C. tropicus*, *R. pseudoumbilicus*, *S. pulchra*, *S. heteromorphus*, reworking |

Journal Pre-proof

1089 **Supplementary Table S2.** A list of fossils determined in the studied samples during the analysis
1090 focused on foraminiferal assemblages. Not mentioned samples were barren.

| Sample | Observations |
|---|---|
| Kol-4-6a | Residue undisturbed by wet sieving (clumps), a significant amount of mica, ? weathered pegmatite – a large quantity of garnet, sterile. |
| Kol-4-6b | The residue contains unwashed gray remnants of very fine-grained claystone (flakes), very micaceous, granules, fragments of sharp-edged quartz crystals, garnet, authigenic pyrite, (?) pyroxene, glauconite, coal material, fish scales;<br>**Foraminifers:** Flat finely agglutinated biserial forms, redeposited tests - *Bolivina*, *Cibicides*, fragments of unknown forms, pyrite tests. Most of the shells are dissolved. If *Bolivina* sp. is *Streptochilus* (the preservation level does not allow unequivocal determination), it could also be derived from the Lower Miocene successions (Karpatian regional Central Paratethys stage). |
| Kol-4-7b | Residue undisturbed by wet sieving consisting of very fine-grained material (flakes), small mica fragments, pyrite, carbonized seeds of conifers (? *Glyptostrobus*).<br>**Foraminifers**: Phantom tests of foraminifera, indeterminate, only the tests of *Globigerina* sp. cf. *bulloides* and ?*Cibicides* were identifiable (lower Middle Miocene, Badenian regional Central Paratethys stage). The tests and a large amount of authigenic framboidal pyrite and Fe oxides might indicate significant dissolution of redeposited shells. It also contains fine-grained agglutinated shells - probably *in situ* (*Lagenammina* and indeterminate - SEM needed) – sourced probably from Badenian redeposits. |
| Kol-4-8a | Brown flakes of unwashed material, glauconite;<br>**Foraminifers:** Tests of forms – *Porosononion* sp. cf. *P. granosum, Nonion* (late Middle Miocene - Sarmatian - redeposition from the lower Middle Miocene, Badenian successions). |
| Kol-4-8b | Sharp-edged fragments of fine-grained material (quartz, carbonates), granules, glauconite, pyrite fillings of burrows.<br>**Foraminifers:** *Nonion* sp. indet., *Elphidium* (?Sarmatian – redeposition from upper Middle Miocene, Sarmatian redeposits). |
| Kol-4-9b | Agglutinated residue material, somewhat coarser clusters, a lot of mica, glauconite, ? volcanic flakes, laminated sediment of very fine-grained material, larger gray and white pebbles, fish bones;<br>**Foraminifers:** *Elphidium hauerinum*, *Nonion biporus* (if *in situ*, indicates late Middle Miocene, Sarmatian age), both are index (zone) fossils of the Sarmatian stage. |
| Kol-4-10a | Fragments of unwashed laminated rock, fine-grained with biotite. |
| Kol-4-11b | Flakes of rock undisturbed by the wet sieving, very finely laminated, biotite, pyrite;<br>**Foraminifers:** Contains very flat, very finely agglutinated (?) *Lagenammina* – typical for marshes (very shallow, extreme environment). |
| Kol-4-12a,b | Fragments of unwashed material, coarser-grained, mica, glauconite, biotite, rhax of sponges, fragments of bivalve shells;<br>**Foraminifers:** *Elphidium hauerinum*, *E. excavatum*, *E. macellum*, *Anoimalinoides cf. dividens*, *Nubecularia sp.* (if *in situ,* indicates upper part of the early Sarmatian age according to Harzhauser and Piller, 2007). |

1091

**Supplementary Table S3 [separately attached file].** Concentrations of selected elements and geochemical parameters included in the comparative analysis of the samples analyzed in this study, and samples from the Danube Basin and its surroundings.

[see the attached file]

**Supplementary Table S4.** Biomarker indices based on selected n-alkanes (m/z 57) and chromatograms showing the distribution of monitored n-alkanes. Explanations: CPI - carbon preference index [(nC25+ nC27+ nC29+ nC31+ nC33)/(nC24+ nC26+ nC28+ nC30+ nC32)+(nC25+ nC27+ nC29+ nC31+ nC33)/(nC26+ nC28+nC30+ nC32+ nC34)]/2 (Bray and Evans 1961); TAR - terrigenous/aquatic ratio (nC27+ nC29+ nC31)/(nC15+ nC17+ nC19) (Bourbonniere and Meyers 1996); ACL21-35 - average chain length (21xnC21+23xnC23+25xnC25+27×nC27+29×nC29+31×nC31+33×nC33+35*nC35)/(nC21+nC23+nC25+nC27+nC29+nC31+nC33+n-C35) (Poynter et al. 1989); Paq - aquatic macrophytes proxy (nC23+nC25)/ (nC23+nC25+nC29+nC31) (Ficken et al. 2000).

| Samples | Stratigraphy | Formations | Depositional systems | Depth (m) | CPI | TAR | $ACL_{21-35}$ | n-alkanes (%) | | |
|---|---|---|---|---|---|---|---|---|---|---|
| | | | | | | | | short | mid | long |
| Kol-4-6a | Pannonian | low. Ivanka | b.floor+HEBs | 2306 | 1,46 | 0,86 | 25,28 | 37 | 38 | 24 |
| Kol-4-7a | Pannonian | low. Ivanka | b.floor+HEBs | 2405 | 1,50 | 0,83 | 25,36 | 38 | 38 | 24 |
| Kol-4-8c | Pannonian | low. Ivanka | b.floor+HEBs | 2451 | 1,36 | 0,52 | 24,65 | 43 | 40 | 17 |
| Kol-4-9b | Sarmatian | Vráble | basin floor | 2509 | 1,59 | 0,91 | 26,44 | 43 | 27 | 29 |
| Kol-4-10b | Sarmatian | Vráble | basin floor | 2559 | 1,16 | 1,80 | 26,78 | 26 | 32 | 41 |
| Kol-4-11b | Sarmatian | Vráble | basin floor | 2598 | 1,46 | 0,80 | 25,61 | 41 | 34 | 25 |

## Highlights:

- First direct evidence of deep-water mud redeposition affecting $^{10}Be/^{9}Be$ dating
- Mud reworking traced by sedimentology, biostratigraphy, inorganic and organic geochemistry
- Middle Miocene mud admixture in Upper Miocene beds causes ~2 Myr age offset
- Hybrid event flows eroded older muds exposed at the bottom of Lake Pannon
- Local reworking dominated during rifting, ending with the post-rift stage

Journal Pre-proof

Journal Pre-proof

**Declaration of interests**

☐ The authors declare that they have no known competing financial interests or personal relationships that could have appeared to influence the work reported in this paper.

☒ The authors declare the following financial interests/personal relationships which may be considered as potential competing interests:

Michal Sujan reports financial support was provided by Slovak Research and Development Agency. Tomas Vlcek reports was provided by NextGenerationEU through the Recovery and Resilience Plan for Slovakia. If there are other authors, they declare that they have no known competing financial interests or personal relationships that could have appeared to influence the work reported in this paper.

Journal Pre-proof